Waveguiding in Photonic Crystals:

An Envelope Approximation Using Multiple Scales Analysis

by
Joyce Poon

A THESIS SUBMITTED IN PARTIAL FULFILLMENT
OF THE REQUIREMENTS FOR THE DEGREE OF
BACHELOR OF APPLIED SCIENCE

DIVISION OF ENGINEERING SCIENCE
FACULTY OF APPLIED SCIENCE AND ENGINEERING
UNIVERSITY OF TORONTO

Supervisor: E. H. Sargent
April 2002

Abstract

Inspired by the envelope approximation commonly applied to semiconductor heterostructures, an analytical approach to study photonic crystal waveguides is presented. By treating the waveguide core as a slowly-varying perturbation in the cladding photonic crystal, multiple scales analysis is used to derive an envelope equation which solves for the propagation constants and frequencies of the guided modes. The envelope approximation is completely general for sufficiently weak perturbations and applies to photonic crystal waveguides of any dimensionality.

The multiple scales approach is verified through comparisons between the envelope approximation and results from full numerical simulations. Heterostructure slab waveguides in three dimensional photonic crystal and a slab waveguide with a homogeneous dielectric core surrounded by photonic crystal cladding are studied. The mode shapes are in excellent agreement with simulations. The computed waveguide dispersion relations agree with simulated results to 1%.

The implications and limitations of the envelope approximation are discussed and quantified by examining the validity of the underlying assumptions in the multiple scales framework. Accurate dispersion relations can be obtained with the envelope approximation even when the assumptions are not completely valid.

With the aim of enabling efficient forward-engineering of photonic crystal waveguides, the envelope approximation eliminates the need for computationally intensive simulations and provides a physically intuitive picture to the understanding of waveguiding phenomena in photonic crystals.

Acknowledgements

I am fortunate to have been in the company of many excellent teachers over the year. I thank Professor Edward Sargent for his help, guidance, and mentorship. I am grateful for the invaluable mathematical insights of Professor Dmitry Pelinovsky of McMaster University. I thank Emanuel Istrate and Mathieu Allard for their patience and assistance. I also thank all the members of the lab for their humour and support.

I thank Mathieu Charbonneau-Lefort of Stanford University for navigating into the territory where my work treks. I thank Navin Bhat of the Physics Department for our discussion on photonic crystal $k \cdot p$ theory.

I thank Professors Sajeev John, John Sipe, and Henry van Driel of the Physics Department, Eli Yablonovitch of UCLA, Axel Scherer and Amnon Yariv of Caltech, and Shanhui Fan of Stanford University for helpful conversations on photonic crystals and for sharing their visions of the future of photonics with me.

"What I do not create, I cannot understand." — R. P. Feynman

Contents

Abstract **ii**

Acknowledgements **iii**

List of Symbols and Abbreviations **vii**

List of Figures **viii**

1 Introduction **1**

1.1 Basic Theory of Photonic Crystals 1

1.2 Fabrication of Photonic Crystals 4

1.3 Photonic Crystal Waveguides 5

1.4 Photonic Crystal Heterostructures 9

1.5 Motivation for the Envelope Approximation 9

1.6 Looking Ahead 10

2 Multiple Scales Analysis **11**

2.1 The Envelope Equation 11

2.2 Looking Ahead 16

3 Exploring the Envelope Equation **17**

3.1 Waveguiding 17

3.2 Single- and Multi-Modedness 21

3.3 Looking Ahead 22

4 Numerical Results: Heterostructure Waveguides **23**

4.1 MIT Photonic Bands 23

4.2 Description of Simulation 24

4.3 Mode Shapes and Dispersion Relations 25

4.4 Looking Ahead 26

5 Waveguides with Homogeneous Cores **33**

5.1 Applying the Envelope Approximation 33

5.2 Implications and Limitations 34

5.3 Looking Ahead 37

6 Numerical Results: Waveguides with Homogeneous Cores **38**

6.1 Description of Simulation 38

6.2 Mode Shapes and Dispersion Relations 39

6.3 Looking Ahead 44

7 Discussion and Conclusion **45**

7.1 Accuracy of the Envelope Assumptions 45

7.2 Future Work 48

7.3 Conclusion 50

A Photonic Crystal $k \cdot p$ Theory **52**

A.1 Operators and Perturbation Ansatz 52

A.2 Perturbation Theory 56

A.3 Looking Ahead 60

Bibliography **61**

List of Symbols and Abbreviations

c	Speed of light
$\mathbf{E}$	Electric field vector
$\mathbf{H}$	Magnetic field vector
$\mathbf{u}$	Electric field Bloch mode vector
$\mathbf{r}$	Position vector
ω	Angular frequency
$\mathbf{k}$	Wavevector
n	Index of refraction
ϵ	Dielectric constant
$\epsilon = n, m$	Dielectric constants of a photonic crystal:
	n corresponds to the spheres, m corresponds to the background
a	Lattice constant
$\chi_{n,m}$	Correlation function between waveguide mode and Bloch mode
TE	Transverse electric
TM	Transverse magnetic
PBG	Photonic bandgap
MPB	MIT Photonic Bands
FDTD	Finite difference time domain

List of Figures

1.1 Waveguide in a two dimensional photonic crystal [6]. 4

1.2 Holey fibre. Light can be guided in the extra hole at the centre of the fibre [7]. 5

1.3 Yablonovite. This structure is made by drilling holes into a ceramic material and exhibits a bandgap at microwave frequencies [9]. 6

1.4 Wood-pile photonic crystal [10]. 6

1.5 Inverse opal photonic crystal [11]. 7

1.6 Square tetragonal spiral structure photonic crystal [17]. 7

1.7 Simulation of a waveguide bend in 2D photonic crystal. Photonic crystal waveguides promise to have low losses around sharp bends [4]. 8

2.1 Photonic crystal heterostructure channel waveguide. The darker spheres have a different index of refraction from the white spheres. The arrow indicates the direction of wave propagation in the waveguide. 12

3.1 Photonic crystal heterostructure slab waveguide. The darker spheres have a different index of refraction from the white spheres. The arrow indicates the direction of wave propagation in the waveguide. 19

3.2 Schematic of core and cladding bands for $\epsilon_{core} > \epsilon_{clad}$. 20

4.1 Comparison of the envelope approximation and numerical simulation results at various propagation wavevectors, k_y. a is the lattice constant. $\epsilon_{core} = 11, 1.1$ and $\epsilon_{clad} = 10, 1$. 27

4.2 Dispersion relation of TE-like modes for the heterostructure waveguide with $\epsilon_{core} = 11, 1.1$ and $\epsilon_{clad} = 10, 1$. 28
4.3 Dispersion relation of TM-like modes for the heterostructure waveguide with $\epsilon_{core} = 11, 1.1$ and $\epsilon_{clad} = 10, 1$. 29
4.4 Comparison of the envelope approximation and numerical simulation results at various propagation wavevectors, k_y. a is the lattice constant. $\epsilon_{core} = 10, 1$ and $\epsilon_{clad} = 11, 1.1$. 30
4.5 Dispersion relation for the heterostructure waveguide with $\epsilon_{core} = 10, 1$ and $\epsilon_{clad} = 11, 1.1$. 31

5.1 Dispersion relations for a heterostructure waveguide with $\epsilon_{core} = 10, 1$ and $\epsilon_{clad} = 11, 1.1$. One of the dispersion relations is calculated using a single band curvature as in our previous analysis. Another one is calculated using different curvatures for the core and cladding photonic crystals. 35

6.1 Slab waveguide with homogeneous dielectric core. The index of the core is higher than the equivalent index of the cladding. The arrow indicates the direction of wave propagation. 39
6.2 Comparison of the envelope approximation and numerical simulation results at $k_y = \pi/a$ for the even modes. a is the lattice constant. $\epsilon_{core} = 2$ and $\epsilon_{clad} = 2.25, 1$. The first even mode shows better agreement between simulation and theory. 40
6.3 Comparison of the envelope approximation and numerical simulation results at $k_y = \pi/a$. a is the lattice constant. $\epsilon_{core} = 2$ and $\epsilon_{clad} = 2.25, 1$. The first odd mode shows better agreement. 41
6.4 Dispersion relation of quasi-TE modes. 42
6.5 Dispersion relation of quasi-TM modes. 43

7.1 Inner product of waveguide mode with bulk photonic crystal modes for $\epsilon_{core} = 10, 1$ and $\epsilon_{clad} = 11, 1.1$ at $k_y = \frac{\pi}{a}$. 47
7.2 Inner product of waveguide mode with bulk photonic crystal modes for $\epsilon_{core} = 11, 1.1$ and $\epsilon_{clad} = 10, 1$ at $k_y = \frac{\pi}{a}$. 47
7.3 Inner product of waveguide mode with field modes of the constituent materials. $\epsilon_{core} = 2$ and $\epsilon_{clad} = 2.25, 1$ at $k_y = \frac{\pi}{a}$. 49
7.4 The lateral portion of the bent is a coupled resonant optical waveguide [47]. The periodic cavities act as a waveguide. 50

Chapter 1

Introduction

Heralded as the "semiconductors of light," photonic crystals have captured the imagination of theorists and experimentalists alike since they were first proposed by John and Yablonovitch independently in 1987 [1, 2]. Photonic crystals have refractive indices that vary periodically in at least two dimensions [3].

We motivate the work presented in this thesis with an overview of the theory of and current state of research in photonic crystals. The purpose and impact of this work are highlighted in the context of the development in photonic crystal research.

1.1 Basic Theory of Photonic Crystals

Photonic crystals are periodic dielectric structures. Much like a one dimensional grating, the periodicity of the dielectric constant in a photonic crystal leads to strong resonant scattering for particular wavelengths of light. The complete inhibition of light propagation in all directions over a specific frequency range is made possible in photonic crystals through a suitable choice of lattice geometries and compositional dielectric materials. Photonic crystals that exhibit this property are termed "photonic bandgap (PBG) materials".

To understand light propagation in photonic crystals and PBGs, we turn to the fundamental laws that govern electromagnetic waves – Maxwell's equations. In a non-magnetic

medium, where the relative permeability is 1, the equations

$$\nabla \times \frac{1}{n^2(\mathbf{r})} \nabla \times \mathbf{H}(\mathbf{r}) = \frac{\omega^2}{c^2} \mathbf{H}(\mathbf{r}) \tag{1.1}$$

$$\nabla \times \nabla \times \mathbf{E}(\mathbf{r}) = n^2(r) \frac{\omega^2}{c^2} \mathbf{E}(\mathbf{r}) \tag{1.2}$$

describe the propagation of a monochromatic wave. The first equation is a vectorial eigenvalue problem, with $\frac{\omega^2}{c^2}$ as the eigenvalue and $\mathbf{H}(\mathbf{r})$ as the eigenvector. Moreover, the operator for the magnetic field, $\nabla \times \frac{1}{n^2(\mathbf{r})} \nabla \times$, is a Hermitian operator, and the magnetic field eigenvectors are orthogonal [4]. Equation (1.1) is the master equation in electromagnetics just as the Schrodinger equation is the master equation in quantum mechanics. Realizing the analogy between quantum mechanics and electromagnetics is extraordinarily powerful, for it not only enables the analysis of electromagnetic problems to access the vast arsenal of tools developed in quantum mechanics, but also illustrates more clearly the parallels and differences between the flow of electrons in semiconductors and light propagation in photonic crystals.

Equation (1.2) has the disadvantage that the operator $\frac{1}{n^2(\mathbf{r})} \nabla \times \nabla \times$ is non-Hermitian, though we employ it as the governing equation in this work [4]. We choose to work with the electric field equation because the analysis is less complicated, and it yields sufficiently good results. For the lower bands, the electric field eigenvectors are almost orthogonal; hence, the electric field operator can be regarded as almost Hermitian, simplifying our derivations significantly.

The solutions of the wave equations (1.1) and (1.2) in periodic media are Bloch modes. We may express a periodic variation in the index of refraction as

$$n^2(\mathbf{r}) = n^2(\mathbf{r} + \mathbf{R}), \tag{1.3}$$

where $\mathbf{R}$ is a translation vector. The electric field modes in such a medium take the form

$$\mathbf{E}(\mathbf{r}) = \mathbf{u}(\mathbf{r}) \exp(i\mathbf{k} \cdot \mathbf{r}), \tag{1.4}$$

where $\mathbf{u}(\mathbf{r}) = \mathbf{u}(\mathbf{r} + \mathbf{R})$ is called a Bloch function. Inside the photonic bandgap, no photon modes exist; therefore, light with a frequency inside the photonic bandgap is localized and spontaneous emission is inhibited [1, 2]. In this sense, the photonic bandgap is "emptier than vacuum" [5]. A light wave is evanescent inside the bandgap, and the wavevector $\mathbf{k}$ is imaginary. We may express the wave as

$$\mathbf{E}(\mathbf{r}) = \mathbf{u}(\mathbf{r}) \exp(-\tilde{\kappa} \cdot \mathbf{r}), \tag{1.5}$$

where $\tilde{\kappa}$ is the decay constant and $1/|\tilde{\kappa}|$ is the characteristic decay length.

The formation of a photonic bandgap is analogous to the formation of a stopband in a quarter-wave stack. A photonic bandgap emerges from the resonant scatterings from the constituent dielectric materials in a unit cell and the macroscopic arrangement of these microscopic units [3]. To distinguish between the two scattering mechanisms, we may consider the conventional quarter-wave stack which consists of alternating dielectric layers each having a thickness equal to a quarter of a wavelength. While the quarter wavelength thickness condition ensures maximum reflection from a single layer, a stopband arises from the resonant Bragg scattering from the linear periodic arrangement of the layers. To form a photonic bandgap, the microscopic resonances from the individual dielectric scatterers, such as the rods or spheres located at each lattice point of the photonic crystal, should be commensurate with the macroscopic resonances from their periodic arrangement [3]. Achieving a complete bandgap requires choosing the appropriate lattice, indices of refraction, and geometries of the constituent dielectric microstructures [3]. In general, materials with high dielectric constants (e.g. semiconductors – Si, GaAs, InP) are required for a bandgap at optical frequencies [3].

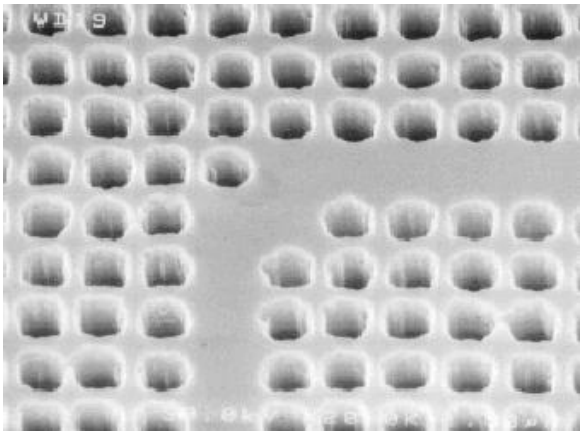

Figure 1.1: Waveguide in a two dimensional photonic crystal [6].

1.2 Fabrication of Photonic Crystals

Breakthroughs in the fabrication, characterization, and modelling of photonic crystals have led to the realizations of a number of photonic crystal structures. Two dimensional photonic crystals are usually fabricated with high resolution electron beam lithography [6]. Commonly, arrays of holes are etched into slabs of semiconductors (figure 1.1). Another type of two dimensional photonic crystal is the holey fibre, consisting of arrays of glass fibres (figure 1.2) [7]. However, two dimensional photonic crystals can only have a bandgap in the plane of periodicity. For a complete bandgap in all directions, three dimensional photonic crystals are needed.

Three dimensional photonic crystals present a greater fabrication challenge. Yablonovitch demonstrated experimentally the existence of a bandgap in microwave frequencies using an inverse diamond structure in a ceramic material (figure 1.3) [8, 9]. This geometry is now known as "Yablonovite." However, the Yablonovite structure could not be readily scaled to optical wavelengths. Another geometry, the wood-pile structure, exploits well-developed semiconductor growth technology and could possess a bandgap near the optical telecommunication wavelength of 1.55μm (figure 1.4) [10]. Two years ago, John *et al.* capitalized on the self-assembly of opal spheres, showing an inverse face-centred-cubic structure in silicon exhibits a complete bandgap at 1.55μm (figure 1.5) [11]. Self-assembly approaches

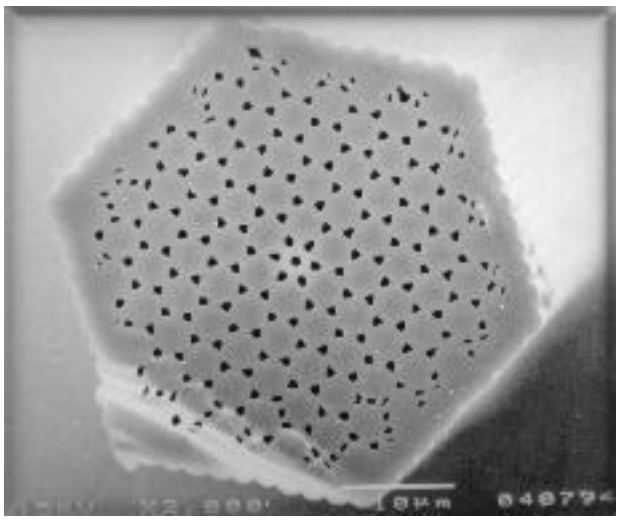

Figure 1.2: Holey fibre. Light can be guided in the extra hole at the centre of the fibre [7].

represent an extensive area of research as achieving long range order remains a critical challenge [12, 13, 14]. Techniques that combine the top-down approach of lithography with the bottom-up approach of self-assembly to enhance ordering of colloidal particles into photonic crystal structures have been demonstrated [15, 16]. Recently, Toader and John proposed a square tetragonal spiral structure which promises to have a large bandgap at 1.55μm (figure 1.6) [17]. Such a structure has been fabricated using glancing angle deposition (GLAD) of silicon though no optical measurements on these photonic crystals are available yet [18].

1.3 Photonic Crystal Waveguides

While the abrupt discontinuity in the density of photon states near a photonic bandgap enables the study of numerous interesting physical phenomena, with engineering practical applications in mind, we focus on the research of functional passive photonic crystal devices, in particular, the photonic crystal waveguide [19].

Waveguides in two dimensional (2D) photonic crystals are well studied. The simplest case begins with a straight slab air waveguide introduced through an air line defect in

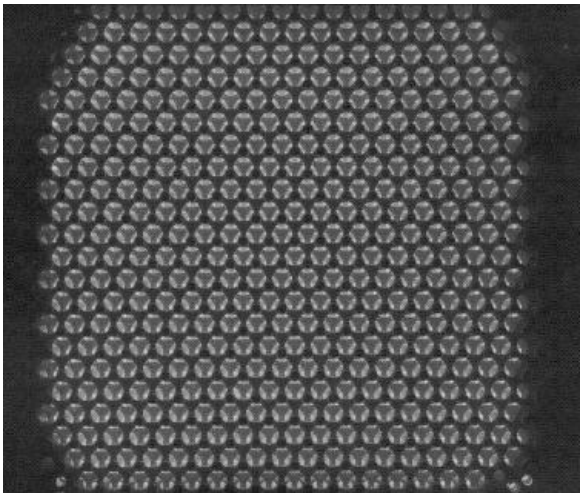

Figure 1.3: Yablonovite. This structure is made by drilling holes into a ceramic material and exhibits a bandgap at microwave frequencies [9].

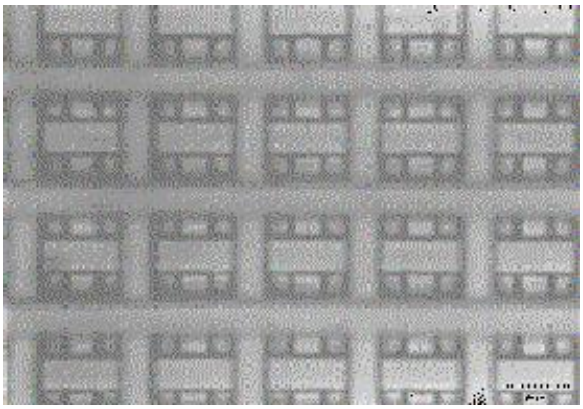

Figure 1.4: Wood-pile photonic crystal [10].

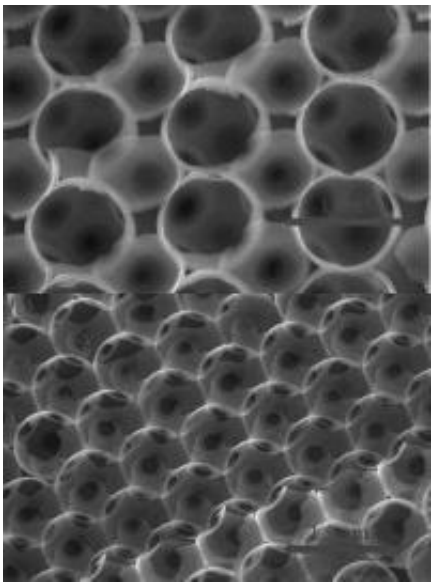

Figure 1.5: Inverse opal photonic crystal [11].

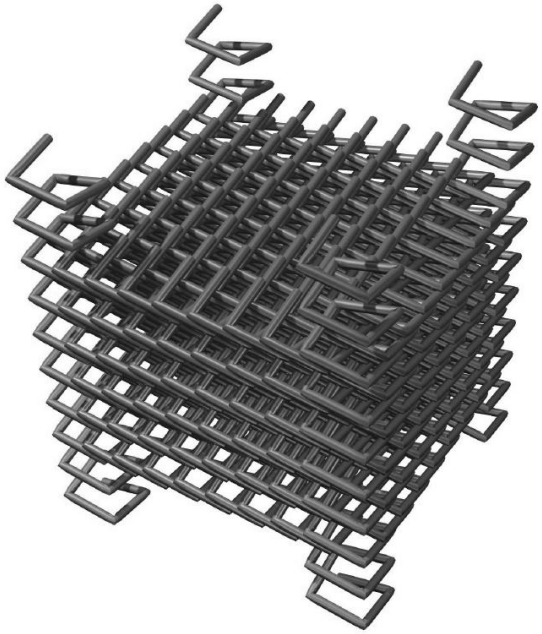

Figure 1.6: Square tetragonal spiral structure photonic crystal [17].

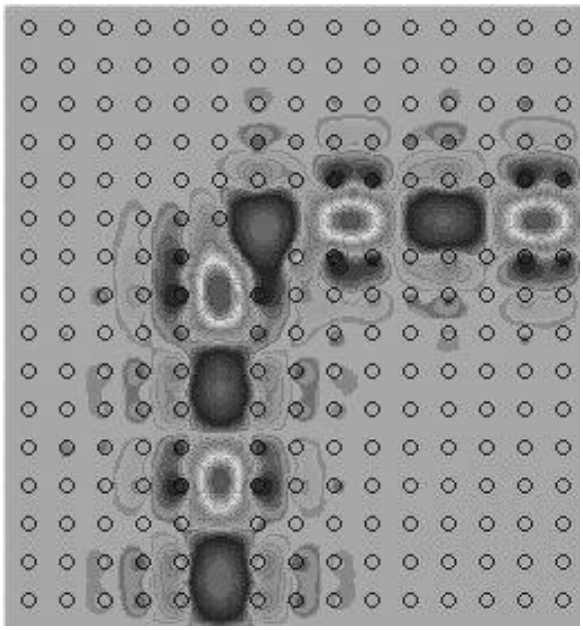

Figure 1.7: Simulation of a waveguide bend in 2D photonic crystal. Photonic crystal waveguides promise to have low losses around sharp bends [4].

2D photonic crystal [4, 20]. More sophisticated variations thereof include the holey fibre, slab dielectric waveguides, and waveguides in photonic crystal slabs, which are finite 2D crystals with index confinement in the third dimension [6, 7, 21, 22]. Investigation into 2D waveguides has mostly been theoretical in nature, focussed on numerical modelling or novel mathematical formalisms such as Wannier function expansions and analytical solutions [23, 24, 25]. These approaches are now used to tackle more application-based problems, such as single- versus multi-mode design and the existence of non-propagating bound states in waveguide bulges [26, 27].

A promised advantage of photonic crystal waveguides over their conventional dielectric counterparts is their ability to confine light even at sharp bends (figure 1.7). Work on bent waveguides has been mostly restricted to 2D crystal structures due to the computational requirements for three dimensional (3D) structures. Most efforts in the theoretical development of bent waveguides have concentrated on numerical methods, and analytical approaches have not been extensively explored [28]. Numerical modelling has been undertaken to study the propagation characteristics at the bends. Greater than 95% trans-

mission around 90 degree bends is predicted [29, 20]. Experiments using microwaves on 90 degree bends verified the aforementioned high transmission efficiency for 2D square lattice of rods and showed a 68% transmission for 3D metallic wood-pile structures [20, 30]. At optical wavelengths, further characterization of bent waveguides awaits, though light has been observed to propagate around 60 degree and 90 degree bends [6, 31].

1.4 Photonic Crystal Heterostructures

In the previous section, we discussed a photonic crystal waveguide in the form of line or planar defects in a bulk photonic crystal. Alternatively, we may introduce a waveguide in the form of a photonic crystal heterostructure. Analogous to semiconductor heterostructures, photonic crystal heterostructures are juxtapositions of different types of photonic crystals. A heterostructure may consist of photonic crystals with different lattice structures, lattice parameters, or indices of refraction.

Photonic crystal heterostructures introduce additional degrees of freedom with which we may tune the properties of photonic crystal devices. In the direction perpendicular to the heterostructure profile, interesting physical phenomena can be studied, and novel devices, such as junctions, filters, and superlattices, may be engineered [32, 33]. In the direction parallel to the heterostructure, the system acts as a waveguide. The photonic heterostructure waveguide is the springboard for the work presented in this thesis.

1.5 Motivation for the Envelope Approximation

Photonic crystals may prove to be crucial ingredients in integrated optics as they enable the design of highly efficient passive and active devices on the same material platform. This thesis develops a formalism for studying photonic crystal waveguides. Just as wires are the pathways for electrons in an electronic chip, photonic crystal waveguides may pave the route for future optical integration.

A key challenge in engineering photonic crystal waveguides is the lack of forward-engineering tools. While these structures can be examined using highly developed simulation techniques, such as plane wave expansion or finite difference time domain methods, such simulations are computationally intensive and cannot by themselves instil a physically intuitive understanding of photonic crystal waveguiding phenomena. Recently, Albert *et al.* proposed a Wannier function expansion approach in the tight-binding approximation to treat point and line defects in two dimensional photonic crystals [23, 24]. Complementing the search for analytical and semi-analytical methods to explain photonic crystal waveguiding, we shall consider waveguides arising from weak perturbations in the bulk photonic crystal and develop an envelope approximation to photonic crystal waveguiding.

1.6 Looking Ahead

Photonic crystals are a novel class of materials that are not only engendering research in fundamental physics, but may also play an important role in optical integration. A major challenge in designing photonic crystal devices is the current dearth of forward-engineering tools. This thesis will show an envelope approximation which addresses the need for an efficient tool and transparent formalism in understanding photonic crystal waveguiding.

Chapter 2

Multiple Scales Analysis

In this chapter, we embark on the derivation of the envelope equation for a photonic crystal heterostructure waveguide. We have previously derived envelope functions through Bloch mode expansions [34]. However, the multiple scales analysis [35] builds on our previous work by providing a transparent and systematic approach in solving the heterostructure waveguide. Our new derivation is a more mathematically rigourous asymptotic expansion. We expect this new analysis can be more easily adaptable to the study of other more complex photonic crystal structures. We will derive a general equation for a channel waveguide in 3D photonic crystal. We shall see our envelope equation is completely analogous to the semiconductor heterostructure envelope equation.

2.1 The Envelope Equation

In the multiple scales method, we separate the photonic crystal heterostructure system into two spatial length scales: the fast-varying scale due to the lattice periodicity of the bulk photonic crystal and the slowly-varying scale due to an index perturbation. We begin with the wave equation

$$\nabla^2\mathbf{E} - \nabla(\nabla\cdot\mathbf{E}) = -\omega_n^2 n^2(\mathbf{r})\mathbf{E}, \tag{2.1}$$

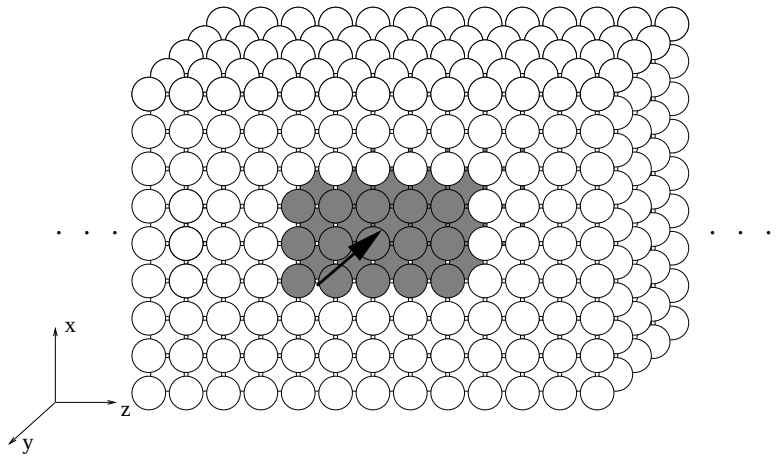

Figure 2.1: Photonic crystal heterostructure channel waveguide. The darker spheres have a different index of refraction from the white spheres. The arrow indicates the direction of wave propagation in the waveguide.

where the speed of light, c, is normalized to 1, and the subscript n labels the eigenfrequency.

We introduce a slowly-varying modulation to the dielectric constant. We adopt the co-ordinates shown in figure 2.1. In Cartesian co-ordinates, the index of refraction is expressed as

$$n^2(x, y, z) = n_0^2(x, y, z) \left[1 + \mu^2 \Delta(X, Z)\right], \tag{2.2}$$

where μ is the perturbation parameter and $\Delta(X, Z)$ is the normalized perturbation. X and Z are the slow variables such that

$$X = \mu x \qquad Z = \mu z. \tag{2.3}$$

Furthermore, we assume that the correction to the eigenvalue, ω_n^2, is

$$\omega_n'^2 = \omega_n^2 + \mu^2 \Omega + \mu^4 \Omega^{(2)} + \ldots \tag{2.4}$$

In (2.2) and (2.4), we set the lowest order perturbation to be of $O(\mu^2)$. Although this choice seems arbitrary at the moment, we shall see that this is necessary for the different

length scales to be compatible in the final equation.

In the spirit of perturbation theory, we assume the solution to the wave equation to be

$$\mathbf{E} = \mathbf{e_0} + \mu \mathbf{e_1} + \mu^2 \mathbf{e_2} + \ldots, \tag{2.5}$$

where $\mathbf{e_i}$ represent the different orders of the expansion. In the multiple scales analysis, we assume that the solution will take the form of a Bloch mode modulated by an envelope function. Hence, we expect the zeroth order term to take the form

$$\mathbf{e_0} = A(X, Z)\tilde{\phi}_{nk}, \tag{2.6}$$

where $A(X, Z)$ is the envelope function and $\tilde{\phi}_{nk}$ is an electric field eigenmode:

$$\tilde{\phi}_{nk} = \exp(i\mathbf{k} \cdot \mathbf{r})|\mathbf{u_{nk}}\rangle, \tag{2.7}$$

where the subscripts k and n label the wavevector and band number respectively. We have also adopted the Dirac notation, treating $\mathbf{u_{nk}}(\mathbf{r})$ as a state function, $|\mathbf{u_{nk}}\rangle$. Since the system is perturbed only in the x and z directions, the envelope should only be a function of these two directions. Analogous to the analysis by de Sterke and Sipe [36], our ansatz for the higher order terms is

$$\begin{aligned} \mathbf{e_1} &= \sum_{l \neq n} B_{lk}(X, Z)\tilde{\phi}_{lk} \\ \mathbf{e_2} &= \sum_{m \neq n} C_{mk}(X, Z)\tilde{\phi}_{mk}, \end{aligned} \tag{2.8}$$

where each order is represented by a sum over the other electric field Bloch modes at the wavevector corresponding to $\tilde{\phi}_{nk}$, with each Bloch mode modulated by an arbitrary envelope function, $B_{lk}(X, Z)$ and $C_{mk}(X, Z)$.

We now proceed to substitute (2.5) into the wave equation to obtain several conditions

on the envelope equation. In the multiple scales method, we treat the slow and fast variables independently. For example, when differentiating, we would write

$$\frac{\partial A}{\partial x} = \mu \frac{\partial A(X,Z)}{\partial X}. \tag{2.9}$$

Therefore, to $O(1)$, we simply have the unperturbed equation. To the next order, $O(\mu)$, we find

$$\begin{aligned}
&\left[\frac{\partial A}{\partial Z}\left(-2\frac{\partial u_x}{\partial z} - i2k_z u_x + ik_x u_z + \frac{\partial u_z}{\partial x}\right) + \frac{\partial A}{\partial X}\left(ik_z u_z + \frac{\partial u_z}{\partial z} + ik_x u_x + \frac{\partial u_y}{\partial y}\right)\right]\hat{x} + \\
&\left[\frac{\partial A}{\partial X}\left(-2\frac{\partial u_y}{\partial x} - 2ik_x u_y + ik_y u_x + \frac{\partial u_x}{\partial y}\right) + \frac{\partial A}{\partial Z}\left(-2\frac{\partial u_y}{\partial z} - 2ik_z u_y + ik_y u_z + \frac{\partial u_z}{\partial y}\right)\right]\hat{y} + \\
&\left[\frac{\partial A}{\partial Z}\left(ik_y u_y + \frac{\partial u_y}{\partial y} + ik_x u_x + \frac{\partial u_x}{\partial x}\right) + \frac{\partial A}{\partial X}\left(-2\frac{\partial u_z}{\partial x} - i2k_x u_z + ik_z u_x + \frac{\partial u_x}{\partial z}\right)\right]\hat{z} + \\
&\sum_{l\neq n} B_{lk}\mathbf{H_0}|\mathbf{u_{nk}}\rangle = 0,
\end{aligned} \tag{2.10}$$

where the action of $\mathbf{H_0}|\mathbf{u_{nk}}\rangle$ is defined in (A.10). Projecting (2.10) to $\frac{1}{V}\langle\mathbf{u_{nk}}|$ and invoking relations (A.23-A.25) yields

$$\left(\frac{\partial A}{\partial Z}\right)\left(\frac{\partial \omega_n^2}{\partial k_z}\right) + \left(\frac{\partial A}{\partial X}\right)\left(\frac{\partial \omega_n^2}{\partial k_x}\right) = 0. \tag{2.11}$$

Since this equality must hold true everywhere and $A(X,Z)$ is not constant in all space (otherwise, we will not have an envelope), we require

$$\frac{\partial \omega_n^2}{\partial k_z} = \frac{\partial \omega_n^2}{\partial k_x} = 0. \tag{2.12}$$

Equation (2.12) stipulates that we must expand about a band extremum in the directions perpendicular to the propagation direction. This condition confirms our intuition about the group velocity of the propagating mode: the components of the group velocity along the transverse directions of the heterostructure profile are zero. The electromagnetic energy of a propagating mode flows parallel to the heterostructure in the direction of the

waveguide core.

From (2.10) we can gain further knowledge about the other envelope functions B_{lk}. Projecting (2.10) to $\frac{1}{V}\langle \mathbf{u_{lk}}|$ and grouping the like terms result in an equation for B_{lk}:

$$B_{lk} = \frac{1}{V}\frac{\frac{\partial A}{\partial X}\langle \mathbf{u_{lk}}|\widetilde{\mathbf{W}}_x|\mathbf{u_{nk}}\rangle + \frac{\partial A}{\partial Z}\langle \mathbf{u_{lk}}|\widetilde{\mathbf{W}}_z|\mathbf{u_{nk}}\rangle}{\omega_l^2 - \omega_n^2}, \tag{2.13}$$

where $\widetilde{\mathbf{W}}_x$ and $\widetilde{\mathbf{W}}_z$ are defined in (A.12 - A.14). These envelope functions will be important in simplifying the final envelope equation.

We shall now tackle the $O(\mu^2)$ terms. When we gather all the $O(\mu^2)$ terms, we find

$$\begin{aligned}
&\left(\frac{\partial^2 A}{\partial Z^2}|\mathbf{u_{nk}^x}\rangle + n^2\Omega A|\mathbf{u_{nk}^x}\rangle + \omega_n^2\Delta n^2 A|\mathbf{u_{nk}^x}\rangle\right)\hat{x} + \\
&\left(\frac{\partial^2 A}{\partial X^2}|\mathbf{u_{nk}^y}\rangle + \frac{\partial^2 A}{\partial Z^2}|\mathbf{u_{nk}^y}\rangle + n^2\Omega A|\mathbf{u_{nk}^y}\rangle + \omega_n^2\Delta n^2 A|\mathbf{u_{nk}^y}\rangle\right)\hat{y} + \\
&\left(\frac{\partial^2 A}{\partial X^2}|\mathbf{u_{nk}^z}\rangle + n^2\Omega A|\mathbf{u_{nk}^z}\rangle + \omega_n^2\Delta n^2 A|\mathbf{u_{nk}^z}\rangle\right)\hat{z} + \\
&\sum_{l\neq n}\left(\frac{\partial B_{lk}}{\partial X}\widetilde{\mathbf{W}}_x|\mathbf{u_{lk}}\rangle + \frac{\partial B_{lk}}{\partial Z}\widetilde{\mathbf{W}}_z|\mathbf{u_{lk}}\rangle\right) + \sum_{m\neq n} C_m\mathbf{H_0}|\mathbf{u_{mk}}\rangle = 0,
\end{aligned} \tag{2.14}$$

where the $|\mathbf{u_{nk}^x}\rangle$, $|\mathbf{u_{nk}^y}\rangle$, and $|\mathbf{u_{nk}^z}\rangle$ are the $\hat{x}$, $\hat{y}$, and $\hat{z}$ components of $\mathbf{u_{nk}}\rangle$ respectively. If we project (2.14) to $\frac{1}{V}\langle \mathbf{u_{nk}}|$ and we substitute B_{lk} from (2.13, we obtain

$$\begin{aligned}
&\frac{\partial^2 A}{\partial X^2}\left(\langle \mathbf{u_{nk}}|\mathbf{u_{nk}}\rangle - \langle \mathbf{u_{nk}^x}|\mathbf{u_{nk}^x}\rangle + \sum_{l\neq n}\frac{|\langle \mathbf{u_{nk}}|\widetilde{\mathbf{W}}_x|\mathbf{u_{lk}}\rangle|^2}{\omega_l^2 - \omega_n^2}\right) + \\
&\frac{\partial^2 A}{\partial Z^2}\left(\langle \mathbf{u_{nk}}|\mathbf{u_{nk}}\rangle - \langle \mathbf{u_{nk}^z}|\mathbf{u_{nk}^z}\rangle + \sum_{l\neq n}\frac{|\langle \mathbf{u_{nk}}|\widetilde{\mathbf{W}}_z|\mathbf{u_{lk}}\rangle|^2}{\omega_l^2 - \omega_n^2}\right) + \Omega A + \omega_n^2\Delta A = 0.
\end{aligned} \tag{2.15}$$

We can further simplify the equation using our relations for the band curvatures. Invoking (A.30) and (A.32), we finally arrive at our envelope equation:

$$\frac{1}{2m_x}\frac{\partial^2 A}{\partial X^2} + \frac{1}{2m_z}\frac{\partial^2 A}{\partial Z^2} + \Omega A + \omega_n^2\Delta(X,Z)A = 0, \tag{2.16}$$

where in analogy to the effective mass in semiconductor physics, we define

$$\frac{1}{m_x} = \frac{\partial^2 \omega_n^2}{\partial k_x^2} \qquad \frac{1}{m_z} = \frac{\partial^2 \omega_n^2}{\partial k_z^2}. \tag{2.17}$$

Equation (2.16) is completely analogous to the envelope equation for semiconductor heterostructures. It also bears resemblance to the time-independent Schrodinger equation. Just like any other partial differential equation, solving (2.16) requires knowledge of the boundary conditions at the interfaces. Solving the envelope equation for a heterostructure waveguide mode is much simpler than solving the full set of Maxwell's equations.

Now we understand why the perturbation to the frequency and dielectric constants are second order (equations 2.2 and 2.4). If they were not of even order, the length scales of the envelope function would not have been μx and μz, since the solution to (2.16) would contain a mixture of scales. We observe that all the terms in (2.16) belong to the same length scales, namely X and Z. Selecting the appropriate scales and correctly identifying the perturbation orders are essential in applying the multiple scales method.

2.2 Looking Ahead

In this chapter, we have used multiple scales analysis to derive an envelope equation applicable to 3D photonic crystals with a 2D heterostructure profile. We have expanded the wave equation using our ansatz for the mode shape, frequency correction, and index perturbation and found an expression for the leading order envelope. The envelope equation is a simple partial differential equation which can be readily solved given the boundary conditions. Our multiple scales method should also work for 3D heterostructure profiles or photonic crystal heterostructure resonators.

Chapter 3

Exploring the Envelope Equation

Not only does the envelope equation simplify the analysis for photonic crystal heterostructure waveguides, it also reveals physical insights into waveguiding phenomena. In this chapter, we will explore the envelope equation to find the conditions for waveguiding and single- or multi-modedness.

3.1 Waveguiding

To solve the two dimensional envelope equation (2.16), we use the technique of separation of variables. We assume $A(X, Z)$ can be written as

$$A(X, Z) = \Psi(X)\Phi(Z). \tag{3.1}$$

We substitute $A(X, Z)$ into the envelope equation to obtain

$$\frac{1}{2m_x}\frac{\Psi"}{\Psi} + \frac{1}{2m_z}\frac{\Phi"}{\Phi} = -(\Omega + \omega_n^2\Delta). \tag{3.2}$$

If we can separate the X and Z dependences such that

$$\Omega + \omega_n^2\Delta = \Xi_x + \Xi_z, \tag{3.3}$$

then Ψ and Φ will satisfy

$$\frac{1}{2m_x}\Psi\text{"} = -\Xi_x\Psi, \tag{3.4}$$

$$\frac{1}{2m_z}\Phi\text{"} = -\Xi_z\Phi. \tag{3.5}$$

For a simple perturbation where the core is described by a constant Δ, centered at the origin, and is $2H$ wide in X and $2L$ wide in Z, the solutions of the equations have the form

$$\begin{aligned}
\Psi(X) &= \begin{cases} F\cos(K_x X) + G\sin(K_x X) & |X| < H \\ Je^{\pm\gamma_x X} & |X| > H \end{cases} \\
\Phi(Z) &= \begin{cases} M\cos(K_z Z) + N\sin(K_z Z) & |Z| < L \\ Pe^{\pm\gamma_z Z} & |Z| > L. \end{cases}
\end{aligned} \tag{3.6}$$

The photonic crystal heterostructure envelope modes are completely analogous to dielectric waveguide modes. The effective mass terms homogenize the photonic crystals and act as an effective index for the photons. We have not discussed how to determine Ξ_x and Ξ_z. In general, much like the channel dielectric waveguide problem, we would employ the effective index method to obtain analytical solutions [37]. However, for the special case of a waveguide with a square cross-section in a cubic lattice, we expect that $\Xi_x = \Xi_z$ due to symmetry considerations. Since the system is invariant under a $\pi/2$ rotation, the band curvatures along x and z should be equal. Therefore, the correction to the eigenfrequency is evenly split between the two directions. The square waveguide in a cubic lattice simplifies to a superposition of two identical slab waveguides in the x and z directions.

To elucidate the waveguiding mechanism, we consider a slab waveguide for which analytical solutions can be readily obtained. The heterostructure profile is along z (figure 3.1). Thus, the envelope equation is

$$\frac{1}{2m_z}\frac{\partial^2 A}{\partial Z^2} + \Omega A + \omega_n^2\Delta(Z)A = 0. \tag{3.7}$$

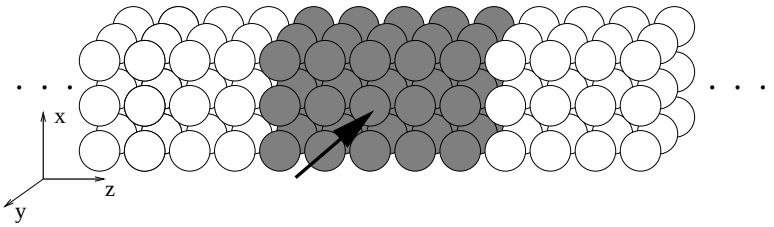

Figure 3.1: Photonic crystal heterostructure slab waveguide. The darker spheres have a different index of refraction from the white spheres. The arrow indicates the direction of wave propagation in the waveguide.

We must expand about a band extremum, where

$$\frac{\partial \omega_n^2}{\partial k_z} = 0. \tag{3.8}$$

For a guide of width $2L$ along Z, the solutions of the envelope equation are

$$A(Z) = \begin{cases} B\cos(KZ) + C\sin(KZ) & |Z| < L \\ De^{\pm\gamma Z} & |Z| > L. \end{cases} \tag{3.9}$$

From these equations, we can determine the condition for waveguiding. For a confined mode, we expect that the mode will decay in the cladding so the curvature of the mode shape is positive. In the core, the mode shape must reach a maximum so the curvature is at some point negative. Assuming that A is positive, the conditions on the curvatures necessitate that Ω and m_z be oppositely signed. This implies Δ and m_z must be of the same sign. Therefore, for real valued γ and K, we can adopt the convention that

$$2m_z(\Delta\omega_n^2 + \Omega) > 0, \tag{3.10}$$

so

$$\gamma \;=\; \sqrt{-2m_z\Omega}$$

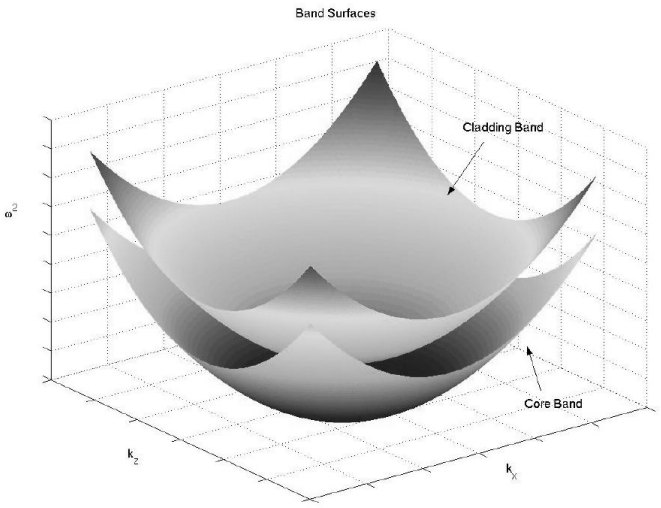

Figure 3.2: Schematic of core and cladding bands for $\epsilon_{core} > \epsilon_{clad}$.

$$K = \sqrt{2m_z(\Delta\omega_n^2 + \Omega)}. \tag{3.11}$$

We conclude that waveguiding occurs when the perturbation in the dielectric function has the same sign as the curvature of the band in the direction perpendicular to the waveguide. We further observe that the guiding frequency will be shifted from the unperturbed frequency by an amount oppositely signed from the dielectric function perturbation.

Figure 3.2 illustrates why this is physically correct. Increasing or decreasing the dielectric constant of a material shifts the dispersion relationship oppositely. For example, a wave of a certain frequency will propagate with a shorter wavevector (longer wavelength) in a material with higher dielectric constant. Furthermore, we recall that waveguiding only occurs when the group velocity in the direction perpendicular to the guide is zero (i.e. $\frac{\partial\omega_n^2}{\partial k_z} = 0$). The band curvature essentially dictates that in the vicinity of this Brillouin zone edge, the frequency allowed in the core is not allowed in the cladding. Therefore, the envelope approximation confirms our intuition about the conditions for waveguiding: a guided wave propagates straight down the core with a frequency allowed in the core but not in the cladding.

3.2 Single- and Multi-Modedness

Since the envelope equation is completely analogous to elementary dielectric waveguide theory, we can readily obtain the single-mode condition. For a slab waveguide, we follow the identical procedure in conventional waveguide analysis [38]. Let us define

$$u = KL \qquad v = \gamma L. \tag{3.12}$$

By enforcing continuity of the envelope and its derivative across the heterostructure interfaces, we obtain the following relationships:

$$\begin{aligned} u\tan u &= v \qquad \text{for even modes} \\ u\tan(u-\pi/2) &= v \qquad \text{for odd modes.} \end{aligned} \tag{3.13}$$

Furthermore,

$$u^2 + v^2 = 2m_z\Delta\omega_n^2 L^2. \tag{3.14}$$

The solutions to u and v, and thus K and γ, are given by the intersections of the curves defined by (3.13) and the circle (3.14). We observe there is always an even mode since the $u\tan u = v$ crosses the origin. Therefore, the single-mode condition requires the radius of the circle be less than $\pi/2$, the onset of the odd mode:

$$0 < |\Delta| < \left|\frac{\pi^2}{8m_z\omega_n^2 L^2}\right|. \tag{3.15}$$

As expected, the wider the waveguide, the weaker must the perturbation be to ensure single-modedness. The band curvature has effectively homogenized the photonic crystal such that $m_z\omega_n^2$ replaces the wavelength and index dependences in the case of conventional dielectric slab waveguide composed of homogeneous materials.

To show the equivalence, we first recall the single-mode condition for a dielectric slab

waveguide:

$$\left(n_2^2 - n_1^2\right) < \frac{\lambda^2}{16L^2}, \tag{3.16}$$

where n_2 and n_1 are the refractive indices of the core and cladding respectively, and $2L$ is the width of the waveguide. If the difference between n_2 and n_1 is small, then we can rewrite (3.16) as

$$\Delta < \frac{\lambda^2}{32\bar{n}L^2} = \frac{\pi^2}{8\bar{n}\omega^2 L^2}, \tag{3.17}$$

where $\Delta = n_2 - n_1$, $\bar{n} = \frac{n_2+n_1}{2}$, and we have normalized c to unity. Comparing this result with (3.15), we see that $\bar{n}$ has been replaced with m_z. The band curvature acts as the reciprocal of a homogenized index for photonic crystal heterostructure waveguides.

3.3 Looking Ahead

The ability to predict the waveguide characteristics and understand the physics underlying the waveguiding phenomena is crucial to the design of photonic crystal waveguides. In this chapter, we have shown how the envelope approximation provides these two ingredients for photonic crystal heterostructure waveguide engineering. We have found the guiding condition and the single-mode condition for a photonic crystal slab waveguide. Through our analysis, we have obtained physical insights into the slope and curvature of a band in the transverse direction. The next step in our investigation is to demonstrate the utility and verify the validity of the envelope approximation by comparing our results with those from the numerical methods commonly employed today.

Chapter 4

Numerical Results: Heterostructure Waveguides

To demonstrate the validity of our envelope approximation, we compare our theoretical results with full numerical simulations of a slab photonic crystal heterostructure waveguide. We use *MIT Photonic Bands* (MPB) software to obtain the band curvatures of the bulk photonic crystal and to find the propagating modes in the heterostructure. We compare the mode shapes and frequencies in waveguides where the average index of the core is greater than that of cladding as well as the converse case.

4.1 MIT Photonic Bands

MPB is a frequency domain eigenvalue solver for photonic crystals [39]. It is capable of computing the bandstructure, electric and magnetic fields, and the electric and magnetic energy densities of an arbitrary photonic crystal. However, the programme assumes a simulation space of an infinitely periodic repetition of a user specified unit cell. Hence, MPB cannot directly solve a sole photonic crystal waveguide where the cladding layers essentially extend infinitely on either side of the core region.

Although this is a serious limitation of MPB, we use this simulator due to the lack

of effective alternatives. An alternative to MPB's frequency domain approach is a finite difference time domain (FDTD) simulation. In FDTD analysis, Maxwell's equations are discretized in time and space and time-stepped to simulate the propagation of the electric and magnetic fields [40]. The simulation space can be arbitrarily defined, and may offer a better representation of the structure we intend to simulate. However, with FDTD simulations, we would not be able to discern a guided mode from the cladding modes since a full bandgap is not necessary for waveguiding in the envelope approximation. FDTD computations are most applicable to finding waveguide modes inside a photonic crystal bandgap. The main advantage of MPB is its capability to generate field intensities at all frequencies within the simulation domain, so we may easily find guided modes from the field patterns.

4.2 Description of Simulation

We use MPB to simulate a slab heterostructure waveguide in three dimensional photonic crystal. The photonic crystal is a cubic lattice of spheres with a radius of $\frac{1}{2}a$, where a is the lattice parameter. We specify our unit cell to consist of a 5 cell wide core and 15 cell wide cladding. We find the 15 cell wide cladding to be sufficiently long to minimize coupling among the adjacent waveguides imposed by the simulator while remaining within our computational capabilities. For the spatial resolution, we choose a grid size of $16 \times 16 \times 16$, such that each cell has 4096 grid points.

To run the simulation, we set y to be the propagation direction and vary k_y in the simulator for a given k_x and k_z. k_z is a band extremum imposed by the envelope approximation. We fix k_x to be 0 in our simulations. The complete dispersion relation of a slab photonic crystal waveguide is a surface, where the propagation frequency is a function of the two propagation vectors, k_x and k_y. Hence, we currently study a particular slice of the surface with $k_x = 0$. Since the unit cell consists of 20 cells in total (5 core and 15 cladding cells), we specify that up to 50 bands be computed for each simulation.

To compare the envelope approximation with the simulated results, we first discriminate the guided modes from the simulation output. We examine the electric field energy densities for all the bands at each wavevector: the energy of a guided wave is concentrated near the core region and evanesces in the cladding. After selecting a guided mode, the envelope function is fitted to a component of the electric field for comparison of the mode shape. We also compare the propagation frequencies predicted by the envelope approximation with those corresponding to the simulation.

4.3 Mode Shapes and Dispersion Relations

Due to the symmetry of the bulk photonic crystal (the cubic lattice of spheres), its first two bands are degenerate. The two degenerate bands correspond to quasi-TE and quasi-TM polarizations, since in the bulk photonic crystal, an electric field polarized along x is equivalent to being polarized along z. We have not accounted for degeneracies in our multiple scales derivation. We shall assume that the envelope functions and predicted dispersion relations are doubly degenerate so both degenerate Bloch modes have the same envelope. This approximation is valid for weak perturbations which do not cause significant splitting of the degenerate eigenstates even if such splitting is present.

The first heterostructure waveguide we examine has a core with an average index higher than that of the cladding. The cladding consists of spheres with a dielectric constant of 10 set in air. We notate the dielectric constants corresponding to the core by $\epsilon_{clad} = 10{,}1$. We consider a Δ of 10%, such that $\epsilon_{core} = 11{,}1.1$. Since Δ is positive, m_z must also be positive. We recall that we must expand about a band extremum or Brillouin zone edge in the transverse direction. From a numerical simulation, we find that $m_z > 0$ at $k_z = 0$.

We generally obtain good agreement between the mode shapes predicted by the envelope approximation and the simulated result. Figure 4.1 shows some representative mode profiles. The envelope function does not match well with the mode profile at $k_y = \pi/a$. The reason for the discrepancy is a breakdown of the envelope approximation, which will be

discussed in chapter 7. Figures 4.2 and 4.3 are the dispersion relations for the waveguide. We observe two distinct guided modes at each wavevector. The exception at $k_y = 0.2\pi/a$ maybe due to the frequency resolution of the simulation software. By checking the field components of the guided modes, we find that the first guided mode is TE-like, with an electric field strongly polarized along x, while the second mode is TM-like, with electric fields strongly polarized along y and z. These two modes are close in frequency and do indeed share a similar envelope. The mode frequencies agree to about 1%.

The second heterostructure waveguide we study switches the core and cladding photonic crystals from the above system, so $\epsilon_{clad} = 11{,}1.1$ and $\epsilon_{core} = 10{,}1$. Consequently, $\Delta = -9.09\%$. For a negative m_z, we find $k_z = \pi/a$. The envelope approximation again agrees well with the simulation results. Figure 4.4 shows the mode shapes, and figure 4.5 shows the dispersion relation. For this simulation, we do not observe the quasi-TM mode. The frequency resolution of MPB is most likely the reason for the discrepancy; the quasi-TE and quasi-TM frequencies are probably too close to be resolved. Again, our predicted mode frequencies agree with the simulated result to about 1%.

4.4 Looking Ahead

In this chapter, we have compared the envelope approximation with full numerical simulations using *MIT Photonic Bands* software. We examine two cases: (1) $\epsilon_{clad} = 10, 1$, $\epsilon_{core} = 11, 1.1$, and (2) $\epsilon_{clad} = 11, 1.1$, $\epsilon_{core} = 10, 1$. Although there are degeneracies in the unperturbed bulk photonic crystal, we assume that the perturbation is weak so any splitting of the degenerate states is minimal. We demonstrate the validity of the envelope approximation as our theoretical results show excellent agreement with the simulation; the mode shapes agree well and the mode frequencies agree to about 1%.

While the study of heterostructure waveguide with a refractive index variation has been fruitful, we seek to extend the envelope approximation to solve more general classes of heterostructures composed of photonic crystals with dissimilar lattice structures. In the

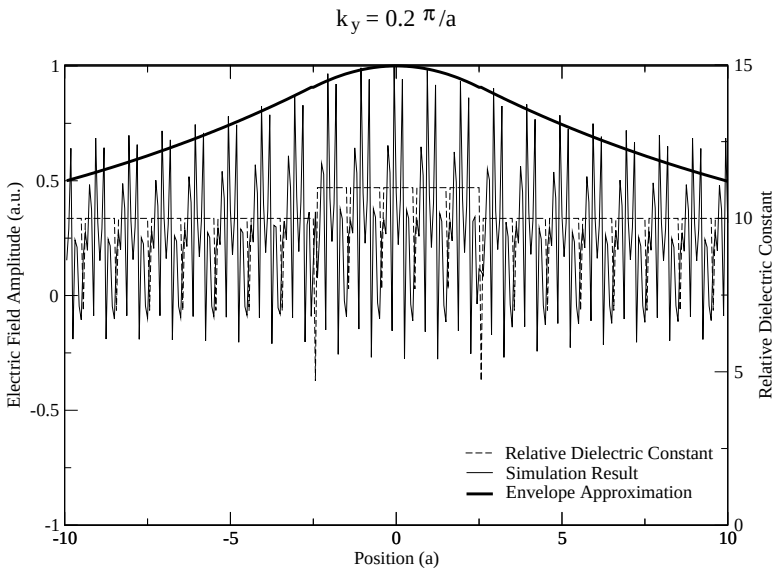

(a)

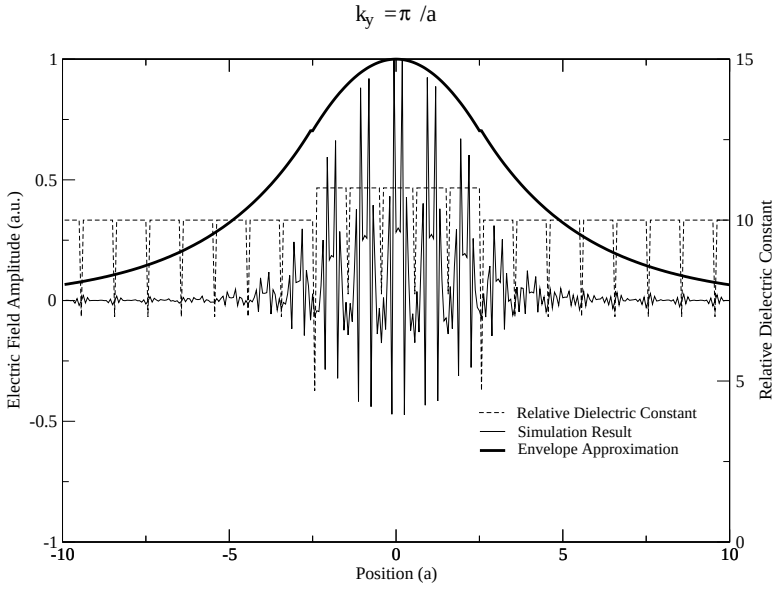

(b)

Figure 4.1: Comparison of the envelope approximation and numerical simulation results at various propagation wavevectors, k_y. a is the lattice constant. $\epsilon_{core} = 11, 1.1$ and $\epsilon_{clad} = 10, 1$.

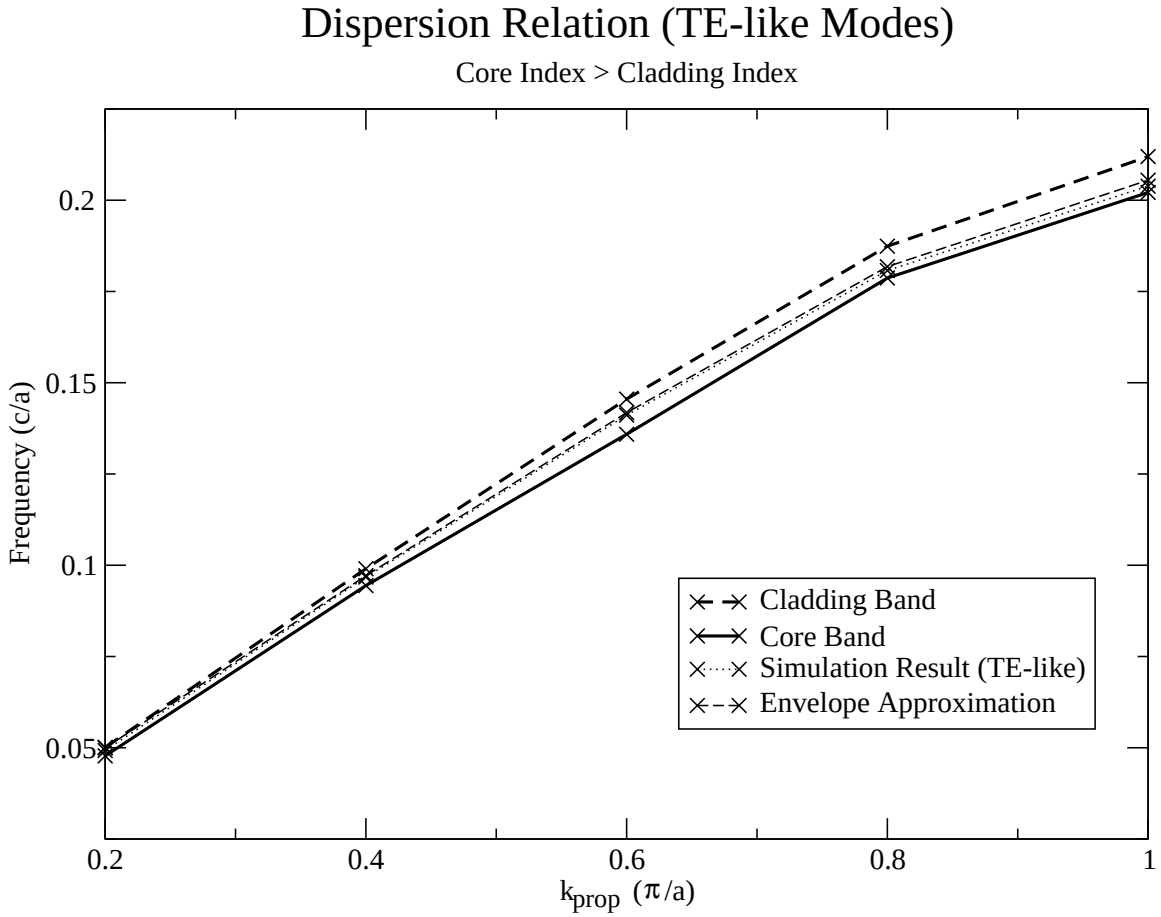

Figure 4.2: Dispersion relation of TE-like modes for the heterostructure waveguide with $\epsilon_{core} = 11, 1.1$ and $\epsilon_{clad} = 10, 1$.

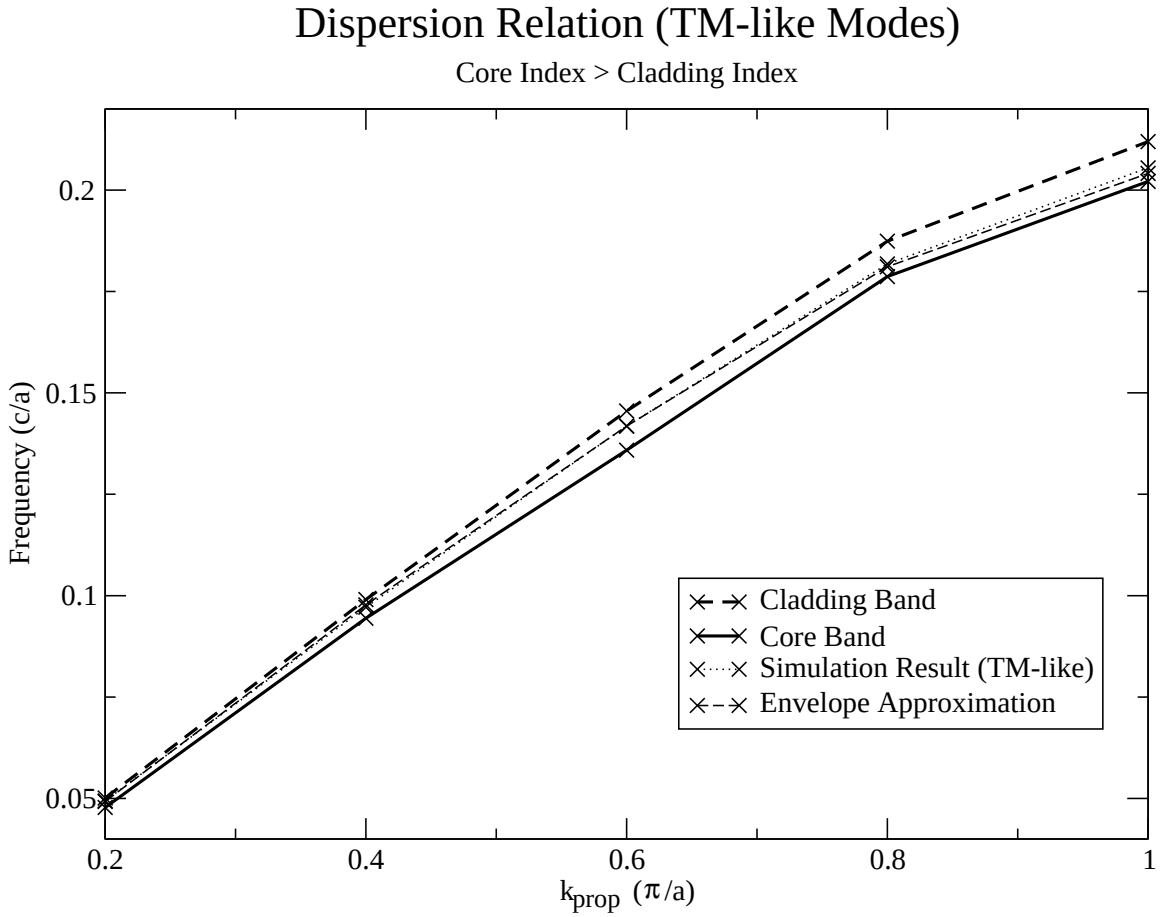

Figure 4.3: Dispersion relation of TM-like modes for the heterostructure waveguide with $\epsilon_{core} = 11, 1.1$ and $\epsilon_{clad} = 10, 1$.

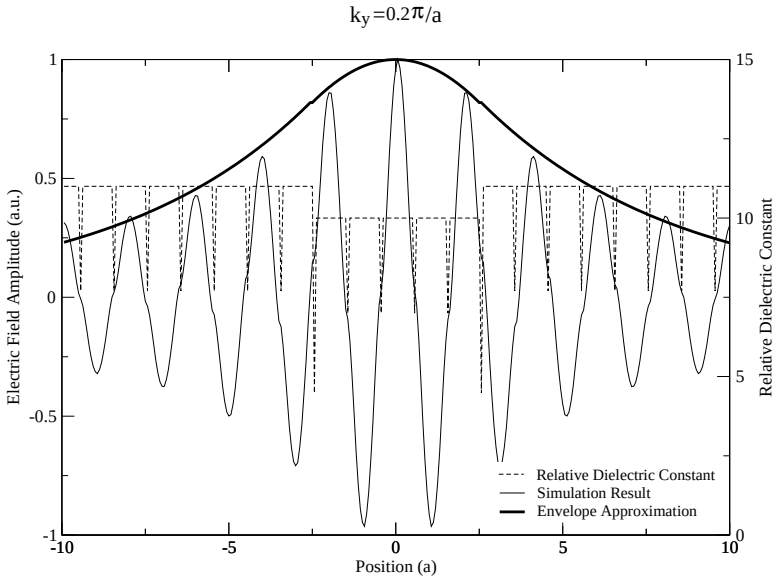

(a)

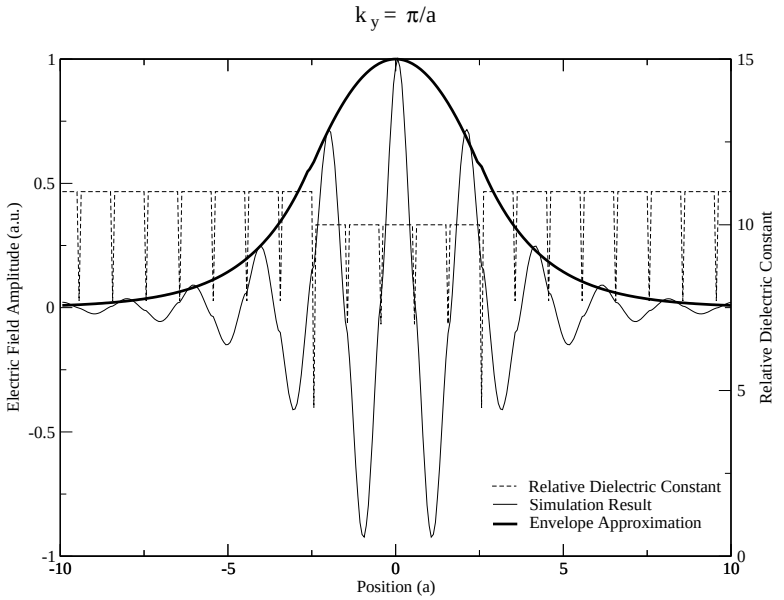

(b)

Figure 4.4: Comparison of the envelope approximation and numerical simulation results at various propagation wavevectors, k_y. a is the lattice constant. $\epsilon_{core} = 10,1$ and $\epsilon_{clad} = 11, 1.1$.

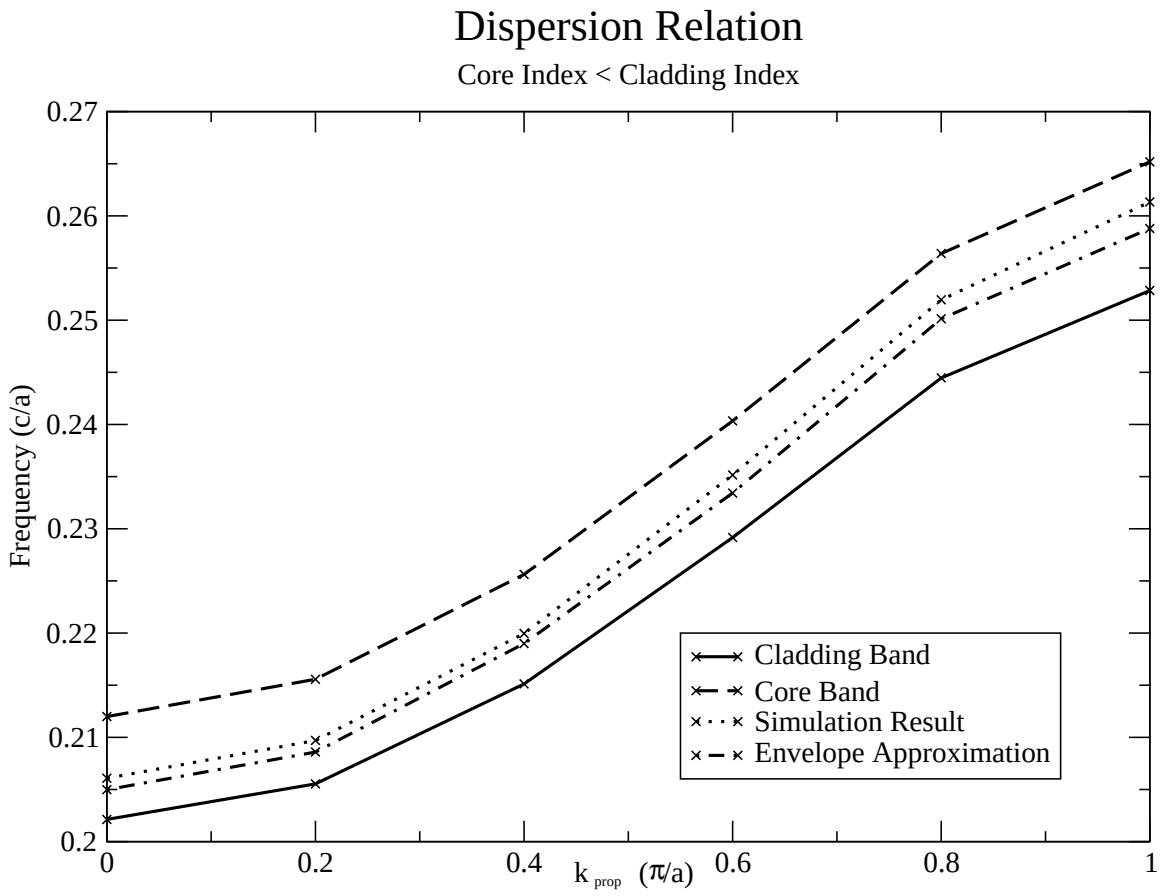

Figure 4.5: Dispersion relation for the heterostructure waveguide with $\epsilon_{core} = 10,1$ and $\epsilon_{clad} = 11, 1.1$.

next chapter, we consider a particular case of such a heterostructure, where the waveguide core consists of a homogeneous dielectric material. The uniform dielectric can be regarded as a crystalline structure with an infinitely small lattice constant.

Chapter 5

Waveguides with Homogeneous Cores

To date, fabricated photonic crystal waveguides are not usually heterostructures with an index modulation as we have discussed so far. Rather, they often consist of a homogeneous dielectric or air core surrounded by a photonic crystal cladding (figures 1.1 and 1.2) [6, 41, 42, 43]. Theoretical work using the tight-binding approximation and coupled mode theory to analyze the conventional photonic crystal waveguides is an active area of research [23, 24, 44]. In this chapter, we will discuss how the envelope approximation complements these approaches in understanding photonic crystal waveguiding.

5.1 Applying the Envelope Approximation

Although the core and the cladding no longer share the same crystalline structure, we begin by assuming that for a guided mode there still exists a set of envelopes that modulates the electric and magnetic fields. For a waveguide with a sufficiently wide homogeneous core, we expect that in a region far away from the core, the envelope will modulate the unperturbed Bloch mode, and in a region near the centre of the core, the envelope will not be modulating any fast variations. For a homogeneous material, the electric field eigenmodes are simply plane waves and thus are associated with constant Bloch functions. Instead of specifying Δ as in (2.2), we assume we can solve the multiple scales problem in the core and cladding

separately. Consequently, we no longer have an effective mass term, m_z or m_x, which is characteristic of only a single type of bulk constituent. We now require a different effective mass term for the cladding and the core.

For a channel waveguide surrounded by photonic crystals, we have two equations that describe the envelope function. The set of equations is

$$\begin{aligned} \frac{1}{2m_{x1}}\frac{\partial^2 A}{\partial X^2} + \frac{1}{2m_{z1}}\frac{\partial^2 A}{\partial Z^2} + \Omega_1 &= 0 \qquad \text{in the cladding} \\ \frac{1}{2m_{x2}}\frac{\partial^2 A}{\partial X^2} + \frac{1}{2m_{z2}}\frac{\partial^2 A}{\partial Z^2} + \Omega_2 &= 0 \qquad \text{in the core,} \end{aligned} \tag{5.1}$$

where the subscripts 1 and 2 denote the quantities associated with the cladding and core respectively, and all the other terms are identically defined in chapter 2. For a slab waveguide parallel to the $x-y$ plane, the envelope function is the solution to

$$\begin{aligned} \frac{1}{2m_{z1}}\frac{\partial^2 A}{\partial Z^2} + \Omega_1 &= 0 \qquad \text{in the cladding} \\ \frac{1}{2m_{z2}}\frac{\partial^2 A}{\partial Z^2} + \Omega_2 &= 0 \qquad \text{in the core.} \end{aligned} \tag{5.2}$$

Although the boundary conditions at the interfaces between crystals with dissimilar lattices remain a subject of contention, we shall assume that the envelope and its derivative are continuous across the boundaries [45]. By enforcing the boundary conditions, we can solve for the envelope function, $A(Z)$.

5.2 Implications and Limitations

By extending the multiple scales derivation, we gain valuable insights into the utility and limitations of the envelope approximation. Our new approach involves solving for the envelope in the core and cladding separately. To test this new approach, we first consider whether it solves the heterostructure waveguide equally well as our previous analysis. We find the new theoretical dispersion relations (figure 5.1) and mode shapes are in good

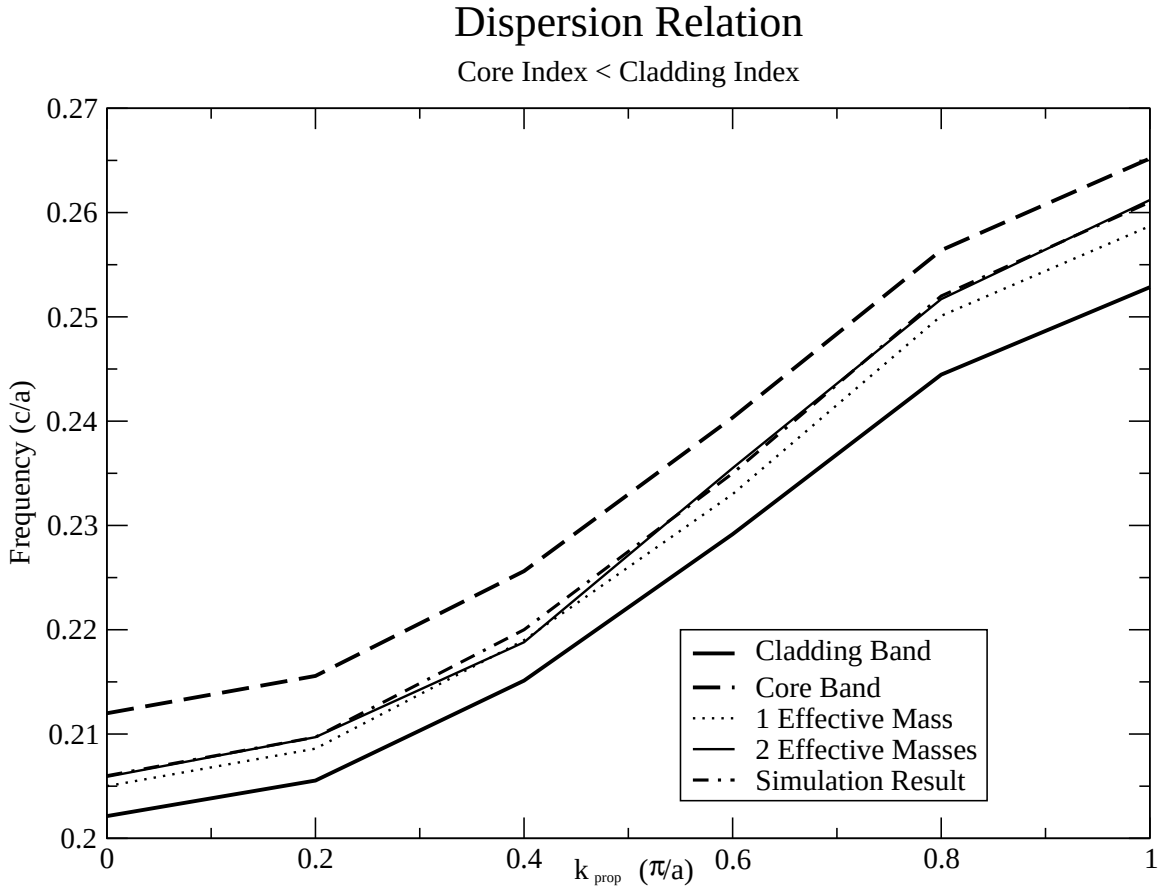

Figure 5.1: Dispersion relations for a heterostructure waveguide with $\epsilon_{core} = 10,1$ and $\epsilon_{clad} = 11, 1.1$. One of the dispersion relations is calculated using a single band curvature as in our previous analysis. Another one is calculated using different curvatures for the core and cladding photonic crystals.

agreement with the previous results.

In a waveguide with a homogeneous core, our envelope equations show regimes where our approximations are no longer valid. The dispersion relation for a homogeneous dielectric is

$$\omega = \frac{k}{n}, \tag{5.3}$$

where $k = \sqrt{k_x^2 + k_y^2 + k_z^2}$ and c is normalized to 1. Thus, we can easily show

$$\frac{\partial \omega^2}{\partial k_z} = 2\frac{k_z}{n^2}, \tag{5.4}$$

and

$$\frac{\partial^2\omega^2}{\partial k_z^2} = \frac{2}{n^2}. \tag{5.5}$$

Our condition that $\frac{\partial\omega^2}{\partial k_z} = 0$ necessitates that we expand about $k_z = 0$. Moreover, the band curvature is constant and positive. Therefore, in our envelope approximation, there will only be guided waves when the band corresponding to the photonic crystal is at a higher frequency than the core band or when the equivalent index of the photonic crystal in the direction of propagation is lower than the index of the core.

But what is the equivalent index? In the last section, we found that the "transverse index," $\bar{n}$, is directly related to $1/\frac{\partial^2\omega^2}{\partial k_z^2}$. However, this relation is not exactly applicable here since the core and cladding materials are different. In our previous analysis of the heterostructure, the single band curvature term homogenizes the photonic crystal "background," so that we isolate the effect of the index perturbation. To compound the confusion, this equivalent index need not be identical to the result from the common empirical formula for photonic crystals:

$$\frac{\epsilon_{eff} - \epsilon_{fill}}{\epsilon_{eff} + 2\epsilon_{fill}} = \beta\frac{\epsilon_{sphere} - \epsilon_{fill}}{\epsilon_{sphere} + 2\epsilon_{fill}}, \tag{5.6}$$

where ϵ_{eff} is the effective dielectric constant, ϵ_{fill} is the dielectric constant of the filling material in the photonic crystal, ϵ_{sphere} is the dielectric constant of the photonic crystal spheres, and β is the volume fill fraction [46].

The answer lies in the shape of the photonic crystal dispersion relation which is related to the dielectric constants, fill fraction, band slope and band curvature. It does not usually have an analytical expression and is computed by solving Maxwell's equations numerically. As long as the photonic crystal band of interest is higher in frequency than the core band, our envelope approximation will predict guided modes.

Lastly, we note that the mode frequency is still expressed as a perturbed quantity of the bulk and cladding materials. Therefore, the core dispersion relation should not deviate too much from that of the cladding. This necessitates that the index of the homogeneous material be similar to the equivalent index of the cladding photonic crystal. The condition

also implies that there is minimum interband mixing. If the homogeneous core is a significant perturbation, we would not be able to assume the modulation of a single Bloch mode by the envelope and our envelope approximation would fail.

Some limitations to the envelope approximation are now obvious. The envelope approximation does not apply to conventional PBG guiding, wherein the frequency of the propagating wave is in the PBG of the cladding photonic crystal but is allowed in the core region. In such a system, the slowly-varying envelope approximation may be invalid, and the index of the core can be lower than that of the cladding. This type of waveguides is best analyzed in the tight-binding approximation [23, 24]. For perturbations that introduce interband or mode mixing, coupled-mode analysis will likely be the most useful [44]. The envelope approximation holds best for weak perturbations with geometric configurations and index contrasts that introduce minimal contributions from other bands.

5.3 Looking Ahead

In this section, we have applied the envelope equation to a photonic crystal waveguide with a homogeneous core. Rather than specifying a fractional index modulation Δ, we solve the envelope equation in the core and cladding separately using a different effective mass, m_z, in each region. We find the envelope approximation is best suited to weak perturbations and does not necessarily apply to PBG guiding. Analogous to the terminology in solid state physics and in contrast to the tight-binding approximation of Albert *et al.*, the envelope approximation is like the "nearly-free photon" approximation for photonic crystal waveguides [23, 24].

Full numerical simulations will verify the validity of solving the envelope equation piecewise in the photonic crystal waveguide. A more in depth examination of our assumptions in the multiple scales derivation will also clarify the applicability of the envelope approximation in arbitrary photonic crystal waveguides.

Chapter 6

Numerical Results: Waveguides with Homogeneous Cores

To test our envelope approximation, we compare our predicted results with full numerical simulations. Much like our previous study of the heterostructure waveguides, we use *MIT Photonic Bands* software for our simulations. Keeping an experimental outlook and complementing concurrent work on colloidal polymeric photonic crystals we select the refractive index of our photonic crystal to match that of para-methoxymethylamphetamine (PMMA) [16].

6.1 Description of Simulation

Similar to the heterostructure waveguides we examined earlier, we study a slab waveguide with a homogeneous dielectric core (figure 6.1). We define a basic unit cell consisting of a 5 cell wide core and 15 cell wide cladding. The cladding is a cubic lattice of spheres in air with radius of $\frac{a}{2}$, where a is the lattice parameter, and a dielectric constant of 2.25 ($\epsilon_{clad} = 2.25, 1$). The dielectric constant of the homogeneous core is 2 ($\epsilon_{core} = 2$). The spatial resolution is set to a grid size of $16 \times 16 \times 16$. We use the same approach to find guided modes and fit envelope functions as in the heterostructure case. Fifty bands are

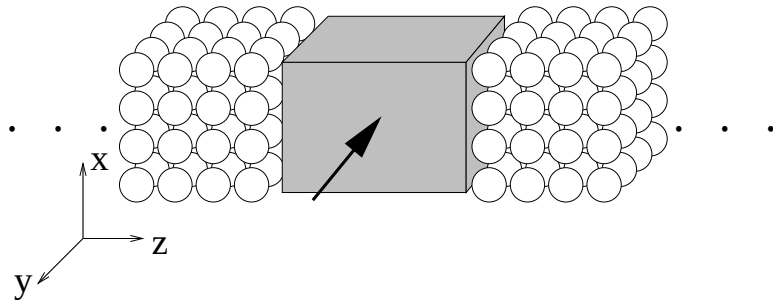

Figure 6.1: Slab waveguide with homogeneous dielectric core. The index of the core is higher than the equivalent index of the cladding. The arrow indicates the direction of wave propagation.

simulated at each wavevector.

6.2 Mode Shapes and Dispersion Relations

For our choice of refractive indices, we generally find good agreement between the envelope approximation and simulated results, except for extra modes arising from additional degeneracies at $k_y = \frac{\pi}{a}$. Figures 6.2 and 6.3 show some representative mode profiles, and figures 6.4 and 6.5 show the dispersion relations for the quasi-TE and quasi-TM polarizations. We see that for almost all the propagation constants, an odd mode exists. This is not too surprising intuitively, as the perturbation in this system is more substantial than the heterostructure.

At $k_y = \frac{\pi}{a}$, several extra modes emerge; these modes do not have counterparts at other propagation vectors. The modes may be caused by the more complicated degeneracies introduced by the homogeneous core. Since a homogeneous material has a continuous dispersion relation, if we neglect polarization dependences and force the dispersion relation to fold back at a Brillouin zone edge, we expect the dispersion relation to be at least doubly degenerate at the zone boundary. Therefore, a cladding mode can be associated with any linear combination of the degenerate core modes. Hence, one envelope function may correspond to at least 4 guided modes as a TE/TM degeneracy is associated with the

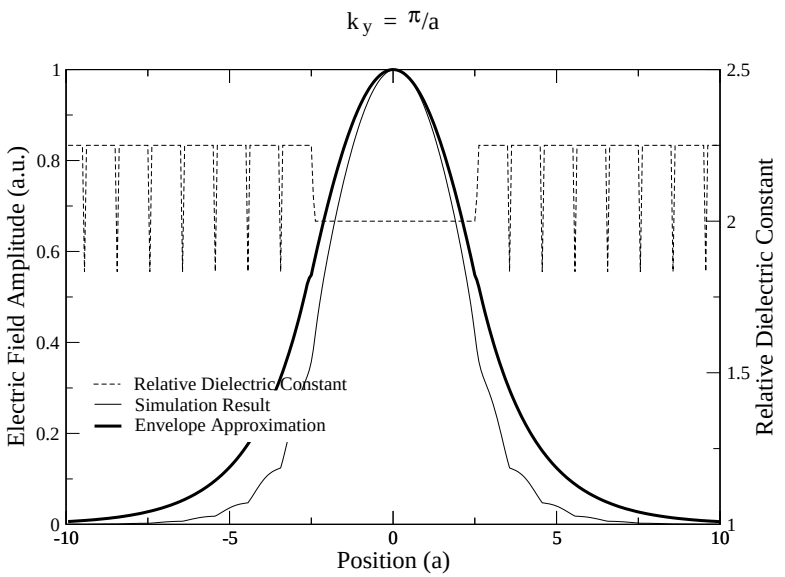

(a) The first even mode at $k_y = \pi/a$.

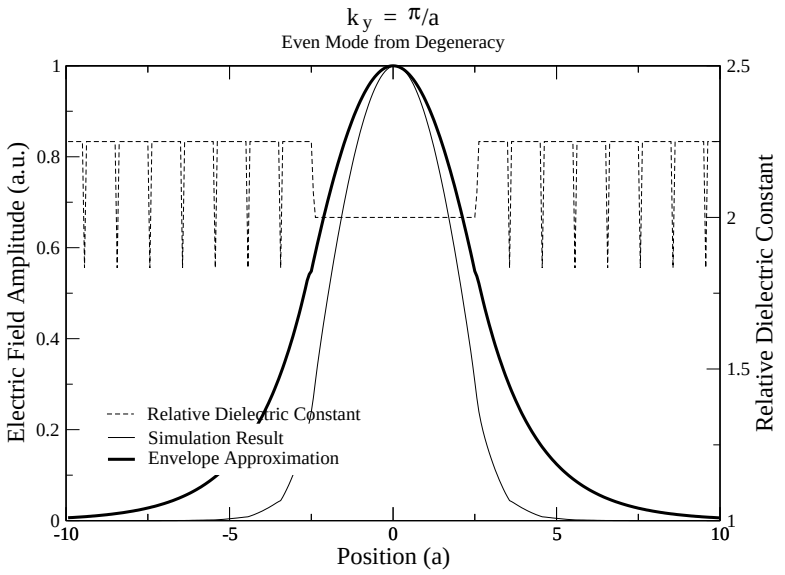

(b) An extra even mode due to degeneracy.

Figure 6.2: Comparison of the envelope approximation and numerical simulation results at $k_y = \pi/a$ for the even modes. a is the lattice constant. $\epsilon_{core} = 2$ and $\epsilon_{clad} = 2.25, 1$. The first even mode shows better agreement between simulation and theory.

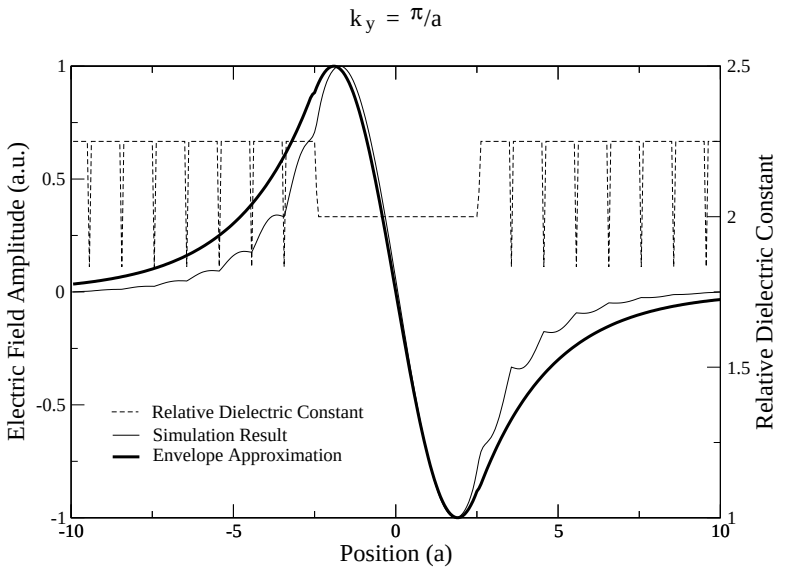

(a) The first odd mode at $k_y = \pi/a$.

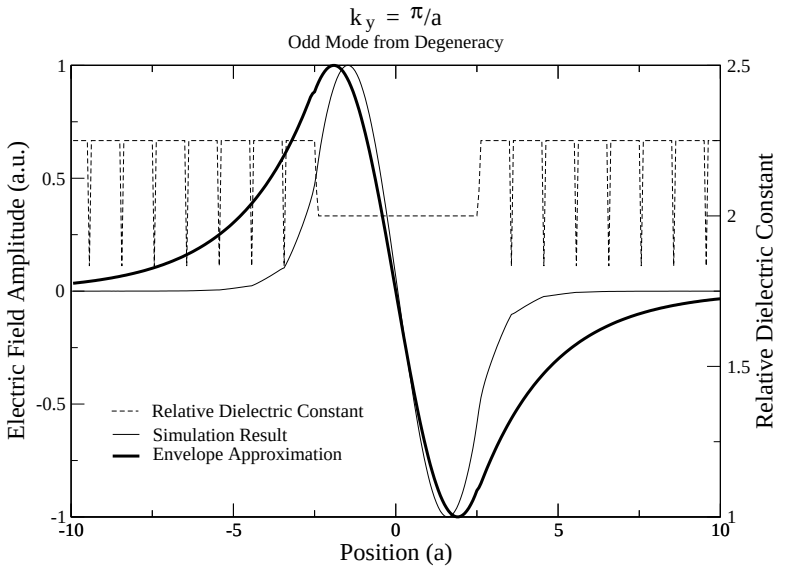

(b) An extra odd mode due to degeneracy

Figure 6.3: Comparison of the envelope approximation and numerical simulation results at $k_y = \pi/a$. a is the lattice constant. $\epsilon_{core} = 2$ and $\epsilon_{clad} = 2.25, 1$. The first odd mode shows better agreement.

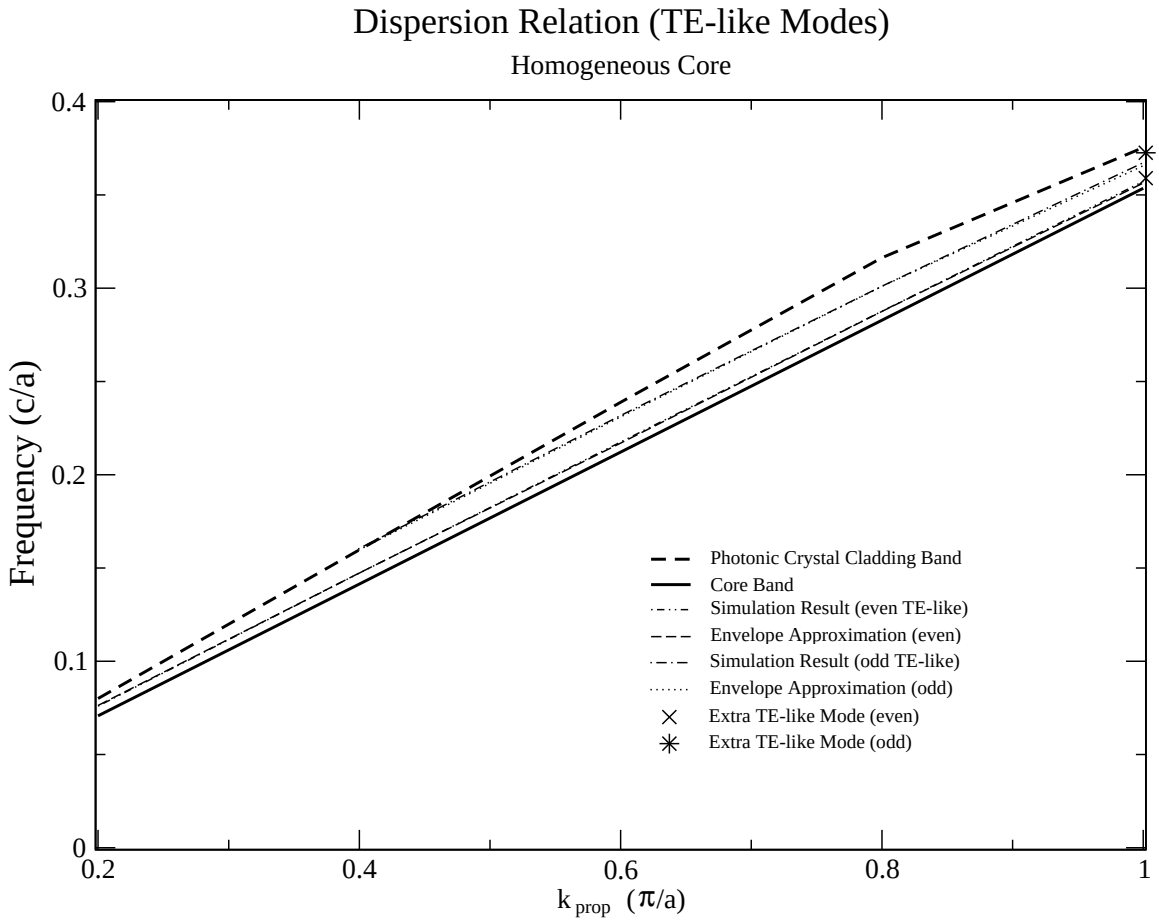

Figure 6.4: Dispersion relation of quasi-TE modes.

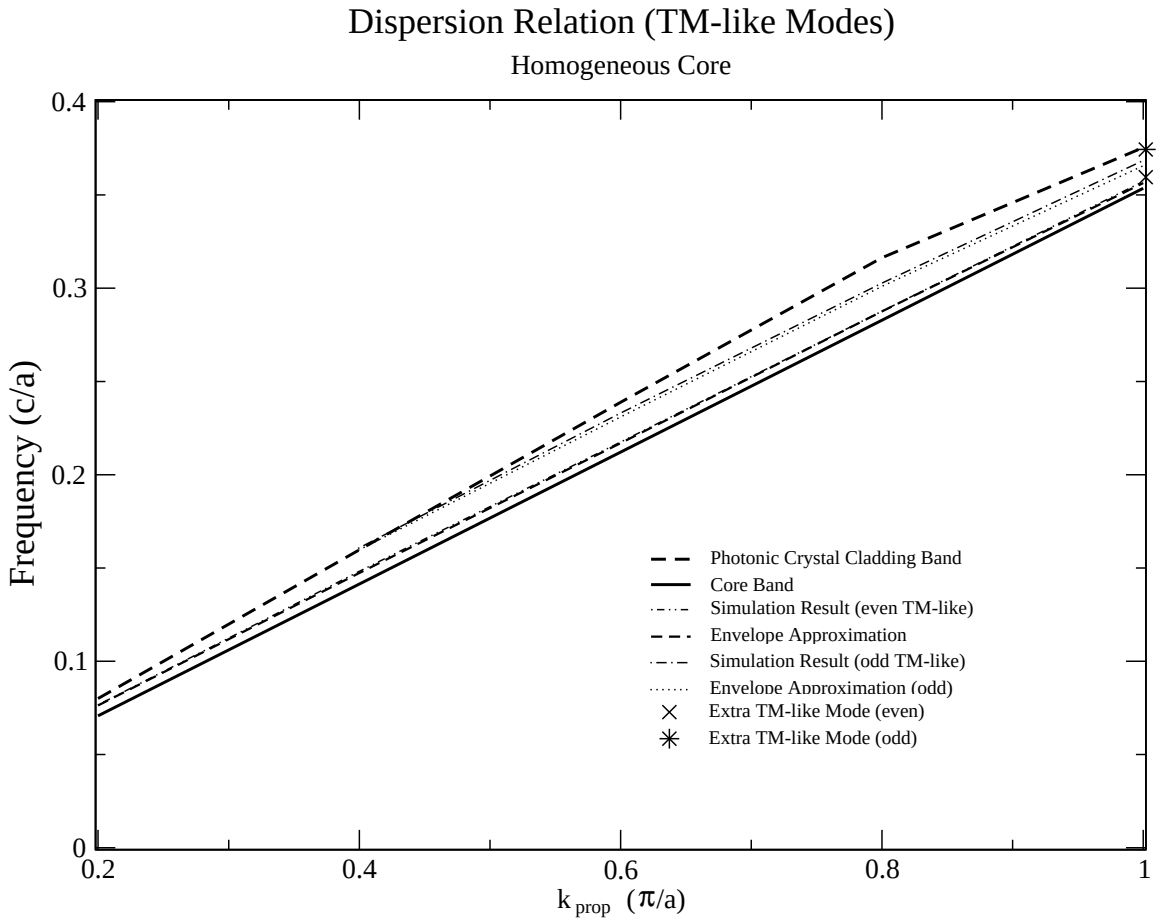

Figure 6.5: Dispersion relation of quasi-TM modes.

photonic crystal as well. Indeed, the simulations show there are 4 even and 4 odd modes at $k_y = \frac{\pi}{a}$. The envelope functions do not fit these extra modes very well (figures 6.2 and 6.3). In chapter 7, we will see that the simulated fields for these modes show low correlation with our assumed form of the mode solution. An examination of the field components reveals these extra modes also have TE-like and TM-like properties.

With the exception of the extra modes, the propagation frequencies from the envelope approximation agree with simulated results to 0.5%. Although we have been able to explain qualitatively the features of the dispersion relations within the envelope picture, in the next chapter, we will quantify the validity of our assumptions and the envelope approximation.

6.3 Looking Ahead

We have extended the envelope approximation to the analysis of a photonic crystal waveguide with a homogeneous dielectric core. We have studied a slab waveguide with $\epsilon_{core} = 2$ surrounded by a cladding of PMMA spheres arranged in a cubic lattice. The mode shapes are generally in excellent agreement, and the mode frequencies agree to within 0.5%. We have not accounted for degeneracy and polarization in the envelope approximation, and we see hints that these effects may lead to a less accurate description of the propagating modes within the envelope formalism. Quantifying the accuracy of the assumptions we have made in the envelope approximation will more clearly define the parameter space where our approach holds best.

Chapter 7

Discussion and Conclusion

We have applied the envelope approximation to the study of photonic crystal waveguides with cores composed of photonic crystals as well as a simple dielectric medium. Implicit in our analysis is the consistency of our envelope approximation – a slowly-varying envelope modulates a Bloch mode. We have also neglected the effects of degeneracies, assuming that the envelope functions can themselves be degenerate. But how accurate are our assertions? How well founded is our envelope conception of waveguide modes? In answering these questions, we gain insights into our envelope approximation that reveal possible avenues for future work.

7.1 Accuracy of the Envelope Assumptions

We quantify the accuracy of our assumption that the envelope modulates a single Bloch mode by defining a correlation function between the waveguide mode and a Bloch mode of the bulk photonic crystal. We seek to determine the correlation between the electric field in each cell of the waveguide structure with Bloch modes of the constituent material, so we may examine how well our envelope approximation holds over the waveguide structure.

We define the correlation function as

$$\chi_{n,m}(z) = |\langle \mathbf{u_{nk}} | \mathbf{\Psi_{mk}} \rangle| \,, \tag{7.1}$$

where we have used the Dirac notation for inner products. $\chi_{n,m}(z)$ is the correlation function which varies along the transverse direction of the waveguide, $|\mathbf{u_{nk}}\rangle$ is an electric field Bloch mode, and $|\mathbf{\Psi_{mk}}\rangle$ is the normalized electric field of a cell in the waveguide. We normalize the electric field in each cell of the waveguide in a similar fashion as the Bloch modes:

$$\langle \mathbf{\Psi_{mk}} | n^2 | \mathbf{\Psi_{mk}} \rangle_{cell} = 1. \tag{7.2}$$

Using the electric fields from the MPB simulations, we compute the correlation functions between all the waveguide modes and the first few bands of the constituent photonic crystal. Figure 7.1 shows $\chi_{n,m}$ as a function of position across the heterostructure waveguide with a lower index in the cladding than the core at $k_y = \frac{\pi}{a}$. $\chi_{1,1}$ is almost equal to 1 over the entire cross-section of the waveguide. The total inner product over the first few bands slightly exceeds unity, which is likely an artifact of the numerical results from the simulations. Nonetheless, the inner product illustrates that only a single Bloch mode is being modulated is an excellent approximation. Therefore, the agreement between the theoretical and computed mode shapes and frequencies is justified.

Although we have just shown a high correlation value leads to good agreement between the envelope approximation and numerical simulation, this is not always the case. For the heterostructure waveguide with a core index higher than cladding index, $\chi_{1,1}$ is about 0.7 (figure 7.2). Although the 70% correlation does not lead to a well-fitting mode envelope (figure 4.1), it is sufficient to obtain agreement in the mode frequency to within 1% (figures 4.2 and 4.3) .

Similar results are obtained for the waveguide with a homogeneous core. For most guided modes, the χ values vary drastically along z, and the maximum of $\chi_{1,1}$ is approx-

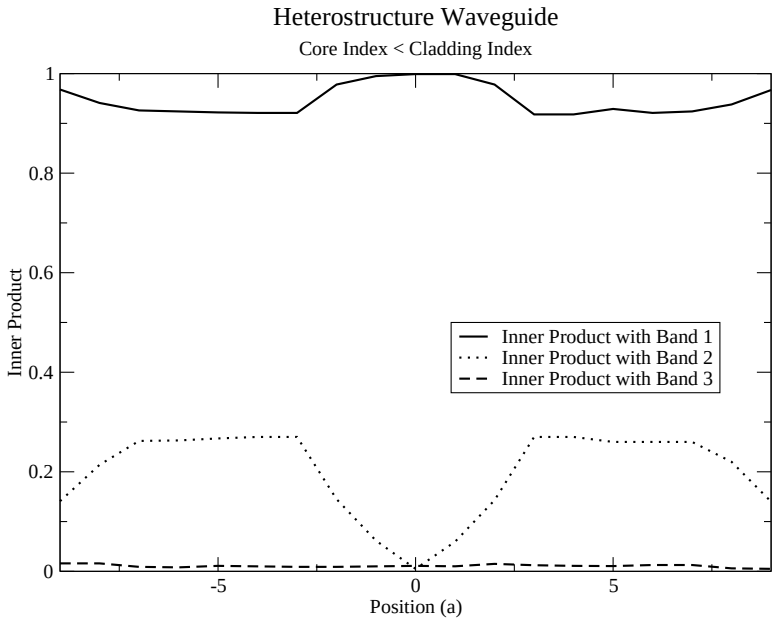

Figure 7.1: Inner product of waveguide mode with bulk photonic crystal modes for $\epsilon_{core} = 10,1$ and $\epsilon_{clad} = 11, 1.1$ at $k_y = \frac{\pi}{a}$.

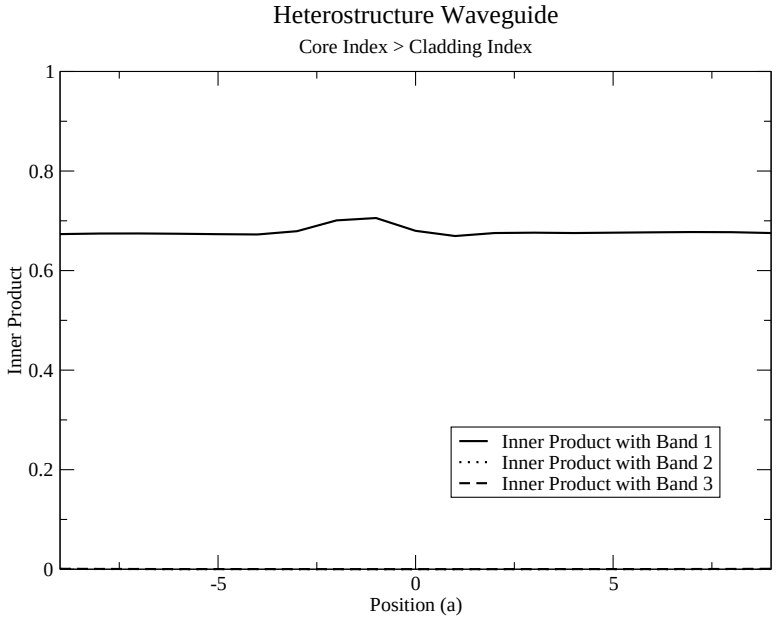

Figure 7.2: Inner product of waveguide mode with bulk photonic crystal modes for $\epsilon_{core} = 11, 1.1$ and $\epsilon_{clad} = 10,1$ at $k_y = \frac{\pi}{a}$.

imately 0.7 (figure 7.3). For the extra mode due to the additional degeneracy associated with $k_y = \frac{\pi}{a}$ (section 6.2), there is significant interband mixing in the cladding region close to the waveguide core. The interband mixing may be due to the degeneracy of the homogeneous dielectric core, coupling among adjacent waveguides in the simulation space, and numerical errors in the simulator. Regardless of the cause of the low correlation, in theory, the envelope approximation should not hold for these modes. However, though the envelope may not fit the field profiles perfectly (figures 6.2 and 6.3), we have managed to account for existence of these modes within our envelope formalism, and our computed mode frequencies agree with the simulated results to better than 2%.

The envelope approximation is robust, as it does not require our assumptions to be absolutely valid to produce acceptably accurate dispersion relations and mode shapes. Our analysis shows good agreement is achieved for $\chi_{n,m} \gtrsim 0.7$. This flexibility implies the envelope approximation may be applicable to the study of a wide range of complex photonic crystal structures which may not satisfy the *a priori* envelope assumptions exactly.

7.2 Future Work

In addition to the photonic crystal waveguides discussed herein, a myriad of opportunities remain. Although our envelope equation is derived for and fully applicable to a channel waveguide, we have not verified our result with numerical simulations due to the lack of an effective computational tool. A simulation technique that solves the three dimensional photonic crystal waveguide will best complement this work. Moreover, to model more realistic three dimensional photonic crystals, such as a face-centred-cubic structure, we may consider adapting our equations to non-orthogonal co-ordinates. In cylindrical co-ordinates, we may derive envelope equations describing wave propagation in curved waveguides.

Furthermore, we can examine photonic crystal resonators using our multiple scales formalism. The resonators may function as filter-type devices. A series of coupled resonators can act as a waveguide, and our analysis will complement the burgeoning work on coupled

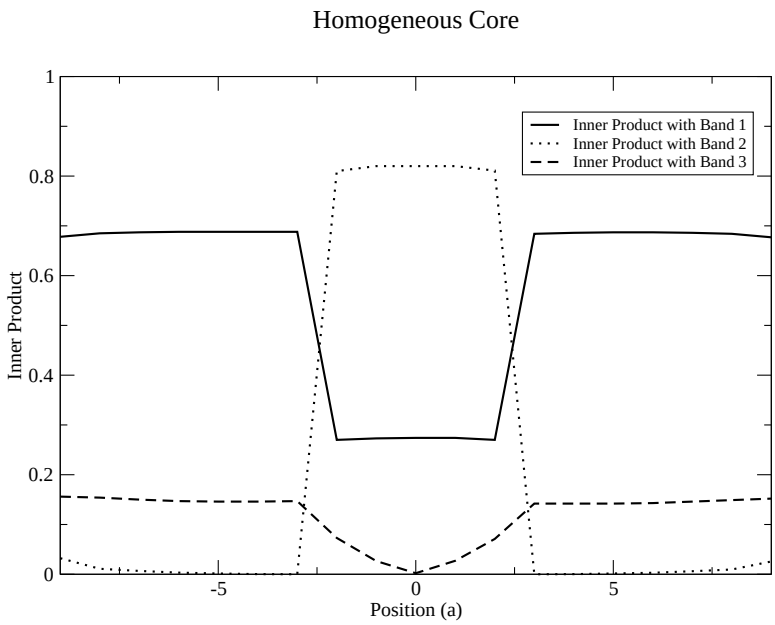

(a) First even mode at $k_y = \frac{\pi}{a}$.

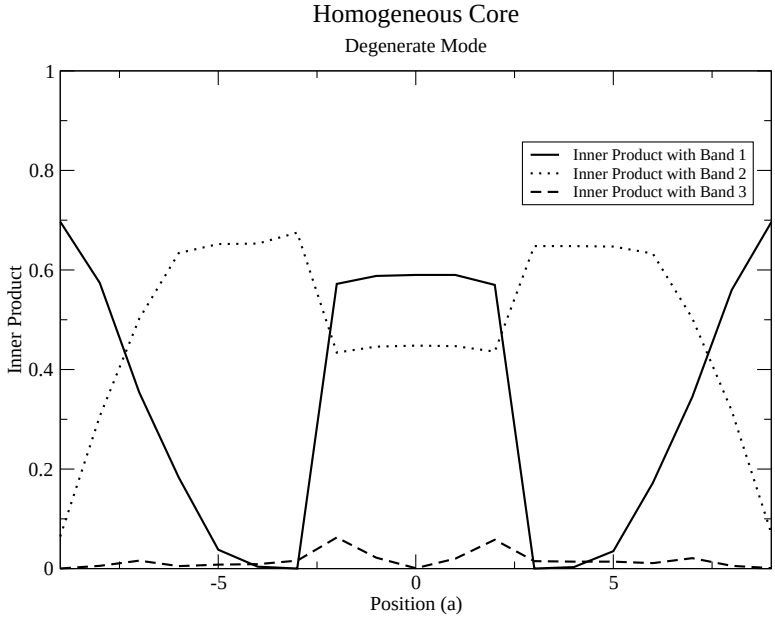

(b) Extra mode due to degeneracy at $k_y = \frac{\pi}{a}$.

Figure 7.3: Inner product of waveguide mode with field modes of the constituent materials. $\epsilon_{core} = 2$ and $\epsilon_{clad} = 2.25, 1$ at $k_y = \frac{\pi}{a}$.

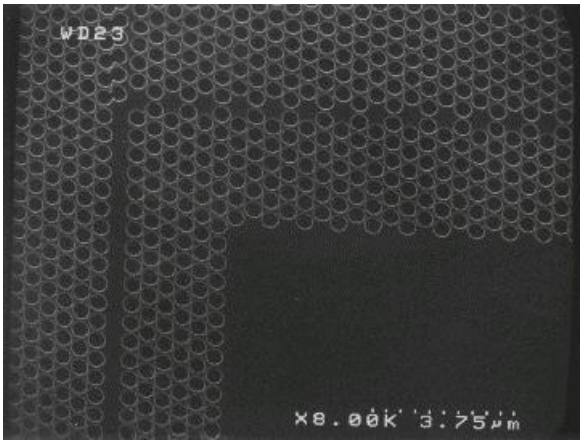

Figure 7.4: The lateral portion of the bent is a coupled resonant optical waveguide [47]. The periodic cavities act as a waveguide.

resonant optical waveguides (CROWs) (figure 7.4) [47, 48]. CROWs show promise in enhancing nonlinear optical effects as the group velocity of a propagating pulse is slowed down in the vicinity of a resonator [48]. Our derivation may be able to incorporate nonlinear interactions since the multiple scales formalism has already been used to study nonlinear photonic crystals [49].

Last but not the least, a physical realization of a photonic crystal heterostructure waveguide and experiments to test our envelope approximation will complete our investigation into photonic crystal heterostructure waveguides. The ultimate aim of the envelope approximation is to facilitate the practical engineering of photonic crystal devices.

7.3 Conclusion

In this thesis, we employ multiple scales analysis to study photonic crystal waveguides. By treating the waveguide core as a slowly-varying perturbation in the cladding photonic crystal, we solve for the propagation constants and frequencies of the waveguide modes. To the leading order, we assume a waveguide mode is a fast oscillating, unperturbed Bloch mode modulated by an envelope which varies on the length scale of the perturbation. Our envelope equation is a partial differential equation analogous to the time-independent

Schrodinger equation. For engineering design applications, we find the single-mode condition for a slab photonic crystal heterostructure waveguide. We discover the band curvatures in the directions perpendicular to the waveguide act as average homogenized refractive indices which account for the photonic crystal.

We demonstrate the validity of our multiple scales method by examining slab waveguides in three dimensional photonic crystals with cores consisting of photonic crystals and a homogeneous dielectric medium. To compare our results with full numerical simulations, we use *MIT Photonic Bands* software to simulate the waveguides. The mode shapes are in good agreement with simulations, and our computed waveguide dispersion relation agrees with simulated results to about 1%.

We explore the limitations and possible extensions of the envelope approximation. The assumptions on which the envelope approximation formalism is founded need not be completely true to obtain accurate results. While fields of the waveguide modes are affected by band degeneracies and subjected to polarization dependences, the envelope approximation supersedes these "microscopic" field properties by describing the modulating functions that encapsulate the general properties of the waveguide modes.

The envelope approximation is an efficient design tool for photonic crystal waveguides, eliminating the computational complexities associated with fully numerical simulations. It also provides a physically intuitive picture to understanding photonic crystal waveguides. The multiple scales method and envelope approximation enhance our mode envelope conception of photonic crystal waveguiding.

Appendix A

Photonic Crystal $k \cdot p$ Theory

Completing the multiple scales expansion requires some results from a $k \cdot p$ theory for photonic crystals. Although more complete and rigourous research on photonic crystal $k \cdot p$ theory has been undertaken to study nonlinearity in photonic crystals, such work cannot be simply or easily applied to our envelope approximation [49, 50]. We shall derive an alternate formulation of the photonic crystal $k \cdot p$ theory that will not only serve our multiple scales expansion but also show the regimes where our envelope approximation will be most applicable.

A.1 Operators and Perturbation Ansatz

We begin with the vector wave equation

$$\nabla \times \nabla \times \mathbf{E} = \frac{\omega_n^2}{c^2} n^2(\mathbf{r}) \mathbf{E}, \tag{A.1}$$

which can be expressed as

$$\nabla^2 \mathbf{E} - \nabla(\nabla \cdot \mathbf{E}) = -\omega_n^2 n^2(\mathbf{r}) \mathbf{E}, \tag{A.2}$$

where we have normalized $c = 1$, and the subscript n labels the eigenfrequency. In a periodic medium, the solutions to the wave equation are

$$\mathbf{E_{nk}}(\mathbf{r}) = \mathbf{u_{nk}}(\mathbf{r}) \exp(i\mathbf{k} \cdot \mathbf{r}), \tag{A.3}$$

where the subscripts n, k label the band and wavevector corresponding to a Bloch mode of the electric field, $\mathbf{u}(\mathbf{r})$. From equation (A.3), we can see that the field operator is of the Sturm-Liouville type, though the eigenvalue, ω_n^2, is multiplied by n^2. Hence, the electric field Bloch modes will satisfy the orthonormality relation

$$\frac{1}{V}\langle \mathbf{u_{mk'}} | n^2 | \mathbf{u_{nk}} \rangle = \delta_{m,n}\delta_{k',k}, \tag{A.4}$$

where we have adopted the Dirac notation, and V is the volume of the cell which fixes the normalization of the Bloch modes. In the derivation that follows, we will use the Dirac notation, treating a Bloch mode, u_{nk}, as a state function, $|\mathbf{u_{nk}}\rangle$.

Now we consider a perturbation in the wavevector to a particular electric field mode, so the new electric field takes the form

$$\mathbf{E'_{nk'}} = \exp(i\mathbf{k'} \cdot \mathbf{r}) |\mathbf{u_{nk'}}\rangle, \tag{A.5}$$

where

$$\mathbf{k'} = \mathbf{k_0} + \mu\tilde{\kappa}. \tag{A.6}$$

μ is the small perturbation parameter, and $\tilde{\kappa}$ is the perturbation wavevector.

Following perturbation analysis, we assume the new Bloch mode will take the form

$$|\mathbf{u_{nk'}}\rangle = |\mathbf{u_{nk}}\rangle + \mu|\mathbf{u_{nk}}^{(1)}\rangle + \mu^2|\mathbf{u_{nk}}^{(2)}\rangle + \ldots, \tag{A.7}$$

where the superscripts denote the orders of the Bloch mode correction. We also assume

the eigenvalue correction is represented by

$$\omega_n'^2 = \omega_n^2 + \mu\lambda^{(1)} + \mu^2\lambda^{(2)} + \ldots, \tag{A.8}$$

where $\lambda^{(n)}$ gives the nth order correction to the eigenvalue.

We substitute our perturbed Bloch mode into the wave equation, and we find

$$(\mathbf{H_0} + \mu\mathbf{W})|\mathbf{u_{nk'}}\rangle = -\omega_n'^2 n^2 |\mathbf{u_{k'}}\rangle, \tag{A.9}$$

where $\mathbf{H_0}$ acts as the unperturbed field operator analogous to a free Hamiltonian in quantum mechanics, while $\mathbf{W}$ is the normalized perturbation operator. However, these operators are complicated by the fact that they are vectorial. By expanding the wave equation in Cartesian co-ordinates, we can define three components ($\hat{x}$, $\hat{y}$, $\hat{z}$) to each vector operator. The action of each component of the vector operator on each component of a Bloch mode (u_x, u_y, u_z) follows explicitly. For example, the $\hat{y}$ component of $\mathbf{H_0}$ is

$$\begin{aligned}\mathbf{H_{0y}}|\mathbf{u_{nk}}\rangle = \frac{\partial^2 u_y}{\partial x^2} + \frac{\partial^2 u_y}{\partial z^2} + 2ik_x\frac{\partial u_y}{\partial x} + 2ik_z\frac{\partial u_y}{\partial z} - k_x^2 u_y - k_z^2 u_y + k_x k_y u_x - \\ ik_x\frac{\partial u_x}{\partial y} + k_z k_y u_z - ik_z\frac{\partial u_z}{\partial y} - ik_y\frac{\partial u_x}{\partial x} - \frac{\partial^2 u_x}{\partial y \partial x} - ik_y\frac{\partial u_z}{\partial z} - \frac{\partial^2 u_z}{\partial y \partial z}.\end{aligned} \tag{A.10}$$

The expression is rather cumbersome due to the curl operator in the original wave equation. Naturally, the other components of $\mathbf{H}_0$ are simply cyclic permutations of the above. Moreover, we observe that $\mathbf{H}_0$ is self-adjoint. Since the corresponding $\mathbf{H}_0$ operator for the electric field is a Sturm-Liouville operator with periodic boundary conditions (A.3), the electric field wave operator is self-adjoint. Changing our basis set from electric field modes to Bloch modes should not alter the self-adjoint property of $\mathbf{H}_0$, thus $\mathbf{H}_0$ as defined in (A.10) is self-adjoint.

Similarly, the $\hat{y}$ component of $\mathbf{W}$ is

$$\begin{aligned}\mathbf{W_y}|\mathbf{u_{nk}}\rangle &= \left(2i\frac{\partial u_y}{\partial x} - 2k_x u_y + k_y u_x - i\frac{\partial u_x}{\partial y}\right)\kappa_x + \\ &\left(k_x u_x - i\frac{\partial u_x}{\partial x} + k_z u_z - i\frac{\partial u_z}{\partial z}\right)\kappa_y + \\ &\left(2i\frac{\partial u_y}{\partial z} - 2k_z u_y + k_y u_z - i\frac{\partial u_z}{\partial y}\right)\kappa_z, \end{aligned} \tag{A.11}$$

where κ_i represents a component of $\tilde{\kappa}$. $\mathbf{W_x}$ and $\mathbf{W_z}$ are also cyclic permutations of $\mathbf{W_y}$. For convenience, we can alternatively define operators $\widetilde{\mathbf{W}}_x$, $\widetilde{\mathbf{W}}_y$, and $\widetilde{\mathbf{W}}_z$, such that

$$\widetilde{\mathbf{W}}_x = \kappa_x \frac{\partial}{\partial \kappa_x}\left(\mathbf{W_x} + \mathbf{W_y} + \mathbf{W_z}\right), \tag{A.12}$$

$$\widetilde{\mathbf{W}}_y = \kappa_y \frac{\partial}{\partial \kappa_y}\left(\mathbf{W_x} + \mathbf{W_y} + \mathbf{W_z}\right), \tag{A.13}$$

$$\widetilde{\mathbf{W}}_z = \kappa_z \frac{\partial}{\partial \kappa_z}\left(\mathbf{W_x} + \mathbf{W_y} + \mathbf{W_z}\right), \tag{A.14}$$

where we have just separated the perturbation dependences of the operators. Therefore,

$$\mathbf{W} = \mathbf{W_x} + \mathbf{W_y} + \mathbf{W_z} = \widetilde{\mathbf{W}}_x + \widetilde{\mathbf{W}}_y + \widetilde{\mathbf{W}}_z. \tag{A.15}$$

A key property of $\mathbf{W}$ is that it is an adjoint operator. In other words, $\langle \mathbf{v_k}|\mathbf{W}|\mathbf{u_k}\rangle = \langle \mathbf{u_k}|\mathbf{W}|\mathbf{v_k}\rangle^*$. This property is a consequence of the periodic nature of Bloch modes. To show this is true, we consider (A.11). For the terms without the derivatives, we note

$$\int_{cell} v_p^* u_q \mathrm{d}V - \left(\int_{cell} u_q^* v_p \mathrm{d}V\right)^* = 0, \tag{A.16}$$

where the subscripts represent the different vector components of $|\mathbf{u_k}\rangle$ and $|\mathbf{v_k}\rangle$. For the terms with the derivatives, we get

$$i\int_{cell} v_p^* \frac{\partial u_q}{\partial r}\mathrm{d}V - \left(i\int_{cell} u_q^* \frac{\partial v_p}{\partial r}\mathrm{d}V\right)^*$$

$$
\begin{aligned}
&= i \int_{cell} \frac{\partial}{\partial r} \left(u_p v_q^* \right) \mathrm{d}V \\
&= 0. \qquad \text{(A.17)}
\end{aligned}
$$

In this section, we define the relevant operators and their action, setting the stage for our $k \cdot p$ derivation. In the next section, we will apply perturbation theory to obtain a relationship between the bandstructure and the Bloch modes.

A.2 Perturbation Theory

Analogous to $k \cdot p$ theory in solid state physics, we shall adopt the same approach as time-independent perturbation theory in quantum mechanics to solve our perturbed system. We shall obtain equations for each order of the perturbation expansion that will relate certain properties of the bandstructure to the Bloch modes.

We begin by substituting the form of the perturbed Bloch mode, wavevector, and eigenfrequency (A.7, A.6, A.8) into the "Hamiltonian" (A.9). We collect terms order by order in μ. For the zeroth order in μ (i.e. $O(1)$), we recover the unperturbed wave equation. To first order, $O(\mu)$, we find

$$
\mathbf{H_0} |\mathbf{u_{nk}}^{(1)}\rangle + \mathbf{W} |\mathbf{u_{nk}}\rangle + \omega_n^2 n^2 |\mathbf{u_{nk}}^{(1)}\rangle + \lambda^{(1)} n^2 |\mathbf{u_{nk}}\rangle = 0. \qquad \text{(A.18)}
$$

Before proceeding, we observe that

$$
\langle \mathbf{u_{nk}} | n^2 | \mathbf{u_{nk}}^{(1)} \rangle = 0, \qquad \text{(A.19)}
$$

because

$$
\langle \mathbf{u_{nk'}} | n^2 | \mathbf{u_{nk'}} \rangle = \langle \mathbf{u_{nk}} | n^2 | \mathbf{u_{nk}} \rangle + \mu \left(\langle \mathbf{u_{nk}} | n^2 | \mathbf{u_{nk}}^{(1)} \rangle + c.c. \right) + \ldots, \qquad \text{(A.20)}
$$

where both $\langle \mathbf{u_{nk'}} | n^2 | \mathbf{u_{nk'}} \rangle$ and $\langle \mathbf{u_{nk}} | n^2 | \mathbf{u_{nk}} \rangle$ are normalized.

When we project (A.18) to $\frac{1}{V}\langle \mathbf{u_{nk}}|$, we obtain

$$\lambda^{(1)} = -\frac{1}{V}\langle \mathbf{u_{nk}}|\mathbf{W}|\mathbf{u_{nk}}\rangle. \tag{A.21}$$

A Taylor expansion about the eigenvalue corresponding to $|\mathbf{u_{nk}}\rangle$ leads to an expression for $\lambda^{(1)}$:

$$\lambda^{(1)} = \kappa_x \frac{\partial \omega_n^2}{\partial k_x} + \kappa_y \frac{\partial \omega_n^2}{\partial k_y} + \kappa_z \frac{\partial \omega_n^2}{\partial k_z}. \tag{A.22}$$

Therefore, simplifying (A.21) and separating the κ_x, κ_y, and κ_z dependences give our first set of relations between the slope at a particular point on the bandstructure to the Bloch mode:

$$\begin{aligned}
\frac{\partial \omega_n^2}{\partial k_x} &= -\frac{1}{V}\int_{cell}\left[u_x^*\left(k_z u_z - i\frac{\partial u_z}{\partial z} + k_y u_y - i\frac{\partial u_y}{\partial y}\right)\right. \\
&\quad + u_y^*\left(2i\frac{\partial u_y}{\partial x} - 2k_x u_y + k_y u_x - i\frac{\partial u_x}{\partial y}\right) \\
&\quad \left. + u_z^*\left(2i\frac{\partial u_z}{\partial x} - 2k_x u_z - i\frac{\partial u_x}{\partial z} + k_z u_x\right)\right] dV
\end{aligned} \tag{A.23}$$

$$\begin{aligned}
\frac{\partial \omega_n^2}{\partial k_y} &= -\frac{1}{V}\int_{cell}\left[u_x^*\left(2i\frac{\partial u_x}{\partial y} - 2k_y u_x + k_x u_y - i\frac{\partial u_y}{\partial x}\right)\right. \\
&\quad + u_y^*\left(k_x u_x - i\frac{\partial u_x}{\partial x} + k_z u_z - i\frac{\partial u_z}{\partial z}\right) \\
&\quad \left. + u_z^*\left(2i\frac{\partial u_z}{\partial y} - 2k_y u_z + k_z u_y - i\frac{\partial u_y}{\partial z}\right)\right] dV
\end{aligned} \tag{A.24}$$

$$\begin{aligned}
\frac{\partial \omega_n^2}{\partial k_z} &= -\frac{1}{V}\int_{cell}\left[u_x^*\left(2i\frac{\partial u_x}{\partial z} - 2k_z u_x + k_x u_z - i\frac{\partial u_z}{\partial x}\right)\right. \\
&\quad + u_y^*\left(2i\frac{\partial u_y}{\partial z} - 2u_y u_z + k_y u_z - i\frac{\partial u_z}{\partial y}\right) \\
&\quad \left. + u_z^*\left(k_y u_y - i\frac{\partial u_y}{\partial y} + k_x u_x - i\frac{\partial u_x}{\partial x}\right)\right] dV.
\end{aligned} \tag{A.25}$$

We can also find the correction to the Bloch mode by projecting (A.18) to another mode at the same k but at a different band, m. We label such as mode as $\langle \mathbf{u_m}|$. The result is

$$n^2|\mathbf{u_{nk}}^{(1)}\rangle = \frac{1}{V}\sum_{m\neq k}\frac{\langle \mathbf{u_{mk}}|\mathbf{W}|\mathbf{u_{nk}}\rangle}{\omega_m^2-\omega_n^2}|\mathbf{u_{mk}}\rangle. \tag{A.26}$$

Since our wave equation did not give pure eigenvalues, and since the electric field modes are orthogonal to each other with respect to the dielectric constant, our eigenvector correction is multiplied by the refractive index.

Now, let us examine the $O(\mu^2)$ terms. This order of the expansion will contain information about the curvature of the band, since the second order correction to the eigenvalue can be written as

$$\lambda^{(2)} = \frac{1}{2}\left(\kappa_x^2\frac{\partial^2\omega_n^2}{\partial k_x^2}+\kappa_y^2\frac{\partial^2\omega_n^2}{\partial k_y^2}+\kappa_z^2\frac{\partial^2\omega_n^2}{\partial k_z^2}+\kappa_x\kappa_y\frac{\partial^2\omega_n^2}{\partial k_x\partial k_y}+\kappa_y\kappa_z\frac{\partial^2\omega_n^2}{\partial k_y\partial k_z}+\kappa_x\kappa_z\frac{\partial^2\omega_n^2}{\partial k_x\partial k_z}\right) \tag{A.27}$$

If we collect all of the second order terms in (A.9) and project the expression to the Bloch mode itself, $\langle \mathbf{u_{nk}}|$, we obtain

$$\begin{aligned}\lambda^{(2)} \;=\; & \frac{1}{V}\Big[\kappa_x^2\left(\langle \mathbf{u_{nk}}|\mathbf{u_{nk}}\rangle-\langle \mathbf{u_{nk}^x}|\mathbf{u_{nk}^x}\rangle\right)+\kappa_y^2\left(\langle \mathbf{u_{nk}}|\mathbf{u_{nk}}\rangle-\langle \mathbf{u_{nk}^y}|\mathbf{u_{nk}^y}\rangle\right)\\ & +\kappa_z^2\left(\langle \mathbf{u_{nk}}|\mathbf{u_{nk}}\rangle-\langle \mathbf{u_{nk}^z}|\mathbf{u_{nk}^z}\rangle\right)+\kappa_x\kappa_y\left(\langle \mathbf{u_{nk}^y}|\mathbf{u_{nk}^x}\rangle+c.c.\right)+\kappa_y\kappa_z\left(\langle \mathbf{u_{nk}^z}|\mathbf{u_{nk}^y}\rangle+c.c.\right)\\ & +\kappa_x\kappa_z\left(\langle \mathbf{u_{nk}^x}|\mathbf{u_{nk}^z}\rangle+c.c.\right)-\sum_{m\neq k}\frac{|\langle \mathbf{u_{mk}}|\mathbf{W}|\mathbf{u_{nk}}\rangle|^2}{\omega_m^2-\omega_n^2}\Big],\end{aligned} \tag{A.28}$$

where $|\mathbf{u_{nk}^x}\rangle$, $|\mathbf{u_{nk}^y}\rangle$, $|\mathbf{u_{nk}^z}\rangle$ are the three vectorial components of the Bloch mode. In arriving at (A.28), we made an important assumption that $|\mathbf{u_{mk}}\rangle$ is orthogonal to $|\mathbf{u_{nk}}\rangle$. This approximation holds true for the lower bands and is verified numerically. The inner product between a Bloch mode from the first few bands and modes of higher bands is about 19 orders of magnitude smaller than its own magnitude. If we did not make the assumption, (A.28) will only be slightly more complicated, where instead of the simple coupling factor,

we will have a term like

$$\sum_{m\neq n} \frac{\langle \mathbf{u_{mk}}|\mathbf{W}/n^2|\mathbf{u_{nk}}\rangle\langle \mathbf{u_{nk}}|\mathbf{W}|\mathbf{u_{mk}}\rangle}{\omega_m^2-\omega_n^2}. \tag{A.29}$$

This is still relatively easy to deal with, but for the sake of simplicity and when analyzing the lower bands, equation (A.28) will suffice.

Following a similar procedure to that used in the $O(\mu)$ analysis, we can separate the terms based on like perturbation parameters to arrive at expressions for the band curvatures:

$$\frac{\partial^2\omega_n^2}{\partial k_x^2} = \frac{2}{V}\left[(\langle \mathbf{u_{nk}}|\mathbf{u_{nk}}\rangle - \langle \mathbf{u^x_{nk}}|\mathbf{u^x_{nk}}\rangle) - \sum_{m\neq n}\frac{|\langle \mathbf{u_{mk}}|\widetilde{\mathbf{W}}_x|\mathbf{u_{nk}}\rangle|^2}{\omega_m^2-\omega_n^2}\right], \tag{A.30}$$

$$\frac{\partial^2\omega_n^2}{\partial k_y^2} = \frac{2}{V}\left[(\langle \mathbf{u_{nk}}|\mathbf{u_{nk}}\rangle - \langle \mathbf{u^y_{nk}}|\mathbf{u^y_{nk}}\rangle) - \sum_{m\neq n}\frac{|\langle \mathbf{u_{mk}}|\widetilde{\mathbf{W}}_y|\mathbf{u_{nk}}\rangle|^2}{\omega_m^2-\omega_n^2}\right], \tag{A.31}$$

$$\frac{\partial^2\omega_n^2}{\partial k_z^2} = \frac{2}{V}\left[(\langle \mathbf{u_{nk}}|\mathbf{u_{nk}}\rangle - \langle \mathbf{u^z_{nk}}|\mathbf{u^z_{nk}}\rangle) - \sum_{m\neq n}\frac{|\langle \mathbf{u_{mk}}|\widetilde{\mathbf{W}}_z|\mathbf{u_{nk}}\rangle|^2}{\omega_m^2-\omega_n^2}\right], \tag{A.32}$$

$$\frac{\partial^2\omega_n^2}{\partial k_x k_y} = \frac{2}{V}\left[(\langle \mathbf{u^y_{nk}}|\mathbf{u^x_{nk}}\rangle + c.c.) - 2\sum_{m\neq n}\frac{Re\left[\langle \mathbf{u_{mk}}|\widetilde{\mathbf{W}}_x|\mathbf{u_{nk}}\rangle\langle \mathbf{u_{mk}}|\widetilde{\mathbf{W}}_y|\mathbf{u_{nk}}\rangle\right]}{\omega_m^2-\omega_n^2}\right], \tag{A.33}$$

$$\frac{\partial^2\omega_n^2}{\partial k_y k_z} = \frac{2}{V}\left[(\langle \mathbf{u^z_{nk}}|\mathbf{u^y_{nk}}\rangle + c.c.) - 2\sum_{m\neq n}\frac{Re\left[\langle \mathbf{u_{mk}}|\widetilde{\mathbf{W}}_y|\mathbf{u_{nk}}\rangle\langle \mathbf{u_{mk}}|\widetilde{\mathbf{W}}_z|\mathbf{u_{nk}}\rangle\right]}{\omega_m^2-\omega_n^2}\right], \tag{A.34}$$

$$\frac{\partial^2\omega_n^2}{\partial k_x k_z} = \frac{2}{V}\left[(\langle \mathbf{u^x_{nk}}|\mathbf{u^z_{nk}}\rangle + c.c.) - 2\sum_{m\neq n}\frac{Re\left[\langle \mathbf{u_{mk}}|\widetilde{\mathbf{W}}_x|\mathbf{u_{nk}}\rangle\langle \mathbf{u_{mk}}|\widetilde{\mathbf{W}}_z|\mathbf{u_{nk}}\rangle\right]}{\omega_m^2-\omega_n^2}\right]. \tag{A.35}$$

We have used our lower band approximation as in (A.28) in arriving at the curvature relations. Our analysis is complete; we can now relate band curvatures to the corresponding Bloch modes.

A.3 Looking Ahead

We have derived a $k \cdot p$ theory for photonic crystals using time independent perturbation theory. We have found the relationships between Bloch modes and the bandstructure. In particular, we have obtained the expressions that relate the slope and curvature at a point on the bandstructure to the Bloch modes corresponding to that wavevector. These results will be useful in simplifying the envelope equations in the multiple scales derivation.

Bibliography

[1] E. Yablonovitch. Inhibited spontaneous emission in solid-state physics and electronics. *Physical Review Letters*, 58(20):2059–2062, 1987.

[2] S. John. Strong localization of photons in certain disordered dielectric superlattices. *Physical Review Letters*, 58(23):2486–2489, 1987.

[3] S. John, O. Toader, and K. Busch. *Photonic bandgap materials, Encyclopedia of Physical Science and Technology*, volume 12, pages 133–145. Academic Press, third edition, 2002.

[4] J. D. Joannopoulos, R. D. Meade, and J. N. Winn. *Photonic Crystals: Molding the Flow of Light*. Princeton University Press, Princeton, 1995.

[5] S. John. Course notes from Advanced Quantum Optics PHY2201S, 2002.

[6] M. Loncar, T. Doll, J. Vuckovic, and A. Scherer. Design and fabrication of silicon photonic crystal optical waveguides. *Journal of Lightwave Technology*, 18(10):1402–1411, 2000.

[7] T. A. Birks, J. C. Knight, B. J. Mangan, and P. St. J. Russell. Photonic crystal fibres: An endless variety. *IEICE Transactions on Communications*, E84-B(5):1211–1218, 2001.

[8] E. Yablonovitch, T. J. Gmitter, and K. M. Leung. Photonic band structures: The face-centered cubic case employing non-spherical atoms. *Physical Review Letters*, 67(17):2295–2298, 1991.

[9] E. Yablonovitch. Photonic crystals: Semiconductors of light. *Scientific American*, 285(6):47–55, 2001.

[10] S. Noda, K. Tomoda, N. Yamamoto, and A. Chutinan. Full three-dimensional photonic bandgap crystals at near-infrared wavelengths. *Science*, 289:604–606, 2000.

[11] A. Blanco and E. Chomski *et al.* Large-scale synthesis of a silicon photonic crystal with a complete three-dimensional bandgap near 1.5 micrometres. *Nature*, 495:437–440, 2000.

[12] Y. A. Vlasov, X. Z. Bo, J. C. Sturm, and D. J. Norris. On-chip natural assembly of silicon photonic bandgap crystals. *Science*, 414:289–293, 2001.

[13] D. J. Norris and Y. A. Vlasov. Chemical approaches to three-dimensional semiconductor photonic crystals. *Advanced Materials*, 13(6):371–376, 2001.

[14] Y-H. Ye, F. LeBlanc, A. Hache, and V-V. Truong. Self-assembling three-dimensional colloidal photonic crystal structure with high crystalline quality. *Applied Physics Letters*, 78(1):52–54, 2001.

[15] G. Ozin and S. M. Yang. The race for the photonic chip: colloidal crystal assembly in silicon wafers. *Advanced Functional Materials*, 11(2):95–104, 2001.

[16] E. Kumacheva, R. K. Golding, M. Allard, and E. H. Sargent. Colloid crystal growth on mesoscopically patterned surfaces: Effect of confinement. *Advanced Materials*, 14(3):221, 2002.

[17] O. Toader and S. John. Proposed square spiral microfabrication architecture for large three-dimensional photonic band gap crystals. *Science*, 292:1133–1135, 2001.

[18] S. Kennedy, M. J. Brett, O. Toader, and S. John. Fabrication of tetragonal square spiral photonic crystals. *Nano Letters*, 2(1):59–62, 2002.

[19] M. Florescu and S. John. Single-atom switching in photonic crystals. *Physical Review A*, 64(3):033801, 2001.

[20] S. Y. Lin, E. Chow, V. Hietala, P. R. Villeneuve, and J. D. Joannopoulos. Experimental demonstration of guiding and bending of electromagnetic waves in a photonic crystal. *Science*, 282(5387):274–276, 1998.

[21] S. G. Johnson, P. R. Villeneuve, S. Fan, and J. D. Joannopoulos. Linear waveguides in photonic-crystal slabs. *Physical Review B*, 62(12):8212–8222, 2000.

[22] A. Adibi, Y. Xu, R. K. Lee, A. Yariv, and A. Scherer. Properties of the slab modes in photonic crystal optical waveguides. *Journal of Lightwave Technology*, 18(11):1554–1564, 2000.

[23] J. P. Albert, C. Jouanin, D. Cassagne, and D. Bertho. Generalized Wannier function method for photonic crystals. *Physical Review B*, 61(7):4318–4384, 2000.

[24] J. P. Albert, C. Jouanin, D. Cassange, and D. Bertho. Photonic crystal modelling using a tight-binding Wannier function method. *Optical and Quantum Electronics*, 32:251–263, 2002.

[25] S. He, M. Popov, M. Qiu, and C. Simovski. An explicit method for the analysis of guided waves in a line-defect channel in a photonic crystal. *Microwave and Optical Technology Letters*, 25(4):236–240, 2000.

[26] A. Adibi, R. K. Lee, Y. Xu, A. Yariv, and A. Scherer. Design of photonic crystal optical waveguides with singlemode propagation in the photonic bandgap. *Electronics Letters*, 36(16):1376–1378, 2000.

[27] A. Mekis, S. Fan, and J. D. Joannopoulos. Bound states in photonic crystal waveguides and waveguide bends. *Physical Review B*, 58(8):4809–4817, 1998.

[28] A. R. McGurn. Photonic crystal circuits. *Phyisca B*, 296(1–3):201–209, 2001.

[29] A. Mekis, J. C. Chen, I. Kurland, S. Fan, P. R. Villeneuve, and J. D. Joannopoulos. High transmission through sharp bends in photonic crystal waveguides. *Physical Review Letters*, 77(18):3787–3790, 1996.

[30] M. Bayindir and E. Ozbay *et al.* Guiding, bending, and splitting of electromagnetic waves in highly confined photonic crystal waveguides. *Physical Review B*, 63(8):1–4, 2001.

[31] T. Baba, N. Fukaya, and J. Yonekura. Observation of light propagation in photonic crystal optical waveguides with bends. *Electronics Letters*, 35(8):654–655, 1999.

[32] E. Istrate and E. H. Sargent. The photonic analogue of the graded heterostructure: Analysis using the envelope approximation. *Optical and Quantum Electronics*, 34:217–226, 2002.

[33] E. Istrate and E. H. Sargent. Photonic crystal heterostructures and the envelope approximation. In *Conference on Lasers and Electro-Optics*, 2002.

[34] M. Charbonneau-Lefort, E. Istrate, M. Allard, J. Poon, and E. H. Sargent. Photonic crystal heterostructures: Waveguiding phenomena and methods of solution in an envelope function picture. *Physical Review B*, 65(12):125318, 2002.

[35] J. Kevorkian. *Partial Differential Equations: Analytical Solutions and Techniques.* Springer, New York, 2000.

[36] C. M. de Sterke and J. E. Sipe. Envelope-function approach for the electrodynamics of nonlinear periodic structures. *Physical Review A*, 38(10):5149–5165, 1988.

[37] H. P. Zappe. *Introduction to Semiconductor Integrated Optics*. Artech House, Boston, 1995.

[38] A. Yariv and P. Yeh. *Optical Waves in Crystals: Propagation and Control of Laser Radiation*. Wiley, New York, 1983.

[39] S. G. Johnson and J. D. Joannopoulos. Block-iterative frequency-domain methods for Maxwell's equations in a planewave basis. *Optics Express*, 8(3):173–190, 2001.

[40] A. Taflove and S. C. Huges. *Computational Electrodynamics: The Finite-Difference Time-Domain Method*. Artech House, Boston, second edition, 2000.

[41] A. Chutinan and S. Noda. Design for waveguides in three-dimensional photonic crystals. *Japanese Journal of Applied Physics*, 39(1 4B):2533–2356, 2000.

[42] C. Weisbuch, H. Benistry, S. Olivier, M. Rattier, C. J. M. Smith, and T. F. Krauss. 3d control of light in waveguide-based two-dimensional photonic crystals. *IEICE Transactions on Communications*, E84-B(5), 2001.

[43] A. Adibi, Y. Xu, R. K. Lee, A. Yariv, and A. Scherer. Guiding mechanisms in dielectric-core photonic-crystal optical waveguides. *Physical Review B*, 64(3):033308, 2001.

[44] A. Yariv. A coupled wave formalism for optical waveguiding by transverse Bragg reflection. *Optics Letters*, 2002. Accepted for publication.

[45] G. Bastard. *Wave Mechanics Applied to Semiconductor Heterostructures*. Halsted Press, New York, 1988.

[46] M. Allard, E. H. Sargent, E. Kumacheva, and O. Kalinina. Characterization of internal order of colloidal crystals by optical diffraction. *Optical and Quantum Electronics*, 34:27–36, 2002.

[47] The Caltech Nanofabrication Group. URL: http://nanofab.caltech.edu.

[48] S. Mookherji and A. Yariv. Coupled resonant optical waveguides. *Journal of Selected Topics in Quantum Electronics*, 8(3), 2002. To be published in June 2002.

[49] N. A. R. Bhat and J. E. Sipe. Optical pulse propagation in nonlinear photonic crystals. *Physical Review E*, 64(5):056604, 2001.

[50] J. E. Sipe. Vector $k{\cdot}p$ approach for photonic band structures. *Physical Review E*, 62(4):5672–5677, 2000.